AESF SUR/FIN '88
Technical Conference Proceedings



AESF

June 27-30, 1988
Los Angeles Convention Center
Los Angeles, CA

88 SUR/FIN

Session I: Electroless Deposition I

American Electroplaters and Surface Finishers Society, Inc.
75th Annual Technical Conference - Los Angeles
Electroless Deposition I
Session I

Electroless Nickel Phosphorus Copper Study in Corrosive Atmospheric Chamber I-1
E. Yang, Saad K Doss
and P. Peterson

Composite Coatings of Fluorinated Carbon (CFx) in Electroless Nickel Plating Bath I-2
Jung T. Kim
Allied-Signal Inc.
Buffalo Research Laboratory
20 Peabody Street
Buffalo, NY 14210

Paper Withdrawn

Corrosion Characteristics of Electroless Nickel Coatings Developed Using Surface Analysis Techniques .. I-3
Lawrence Salvati, Jr.
Perkin-Elmer Corporation
Edison, NJ

Diane M. Tramontana
Occidental Chemical Corporation
Grand Island, NY

Electric Properties of Electroless Copper Deposits I-4
Kuniaki Ohtsuka
Okuno Chemical Industries Co., Ltd.
10-25 1-chome Hanatenhigashi, Tsurumiku
Osaka Japan

Some Physical Properties of Electroless Ni-P Alloy Deposited from Pyrophosphate Bath I-5
Masao Matsuoka, Shinji Imanishi and Tadao Hayashi
Department of Applied Chemistry
University of Osaka Prefecture
4-804 Mozu-Umemachi, Sakai
Osaka, 591, Japan

Advanced Process Control Methods for Electroless Plating of Plastics I-6
Gary Shawhan, Edwin Bastenbeck and Richard Bellemare
Enthone, Inc.
350 Frontage Rd.
West Haven, CT 06516

I-1

Electroless Deposition I
Session I

Electroless Nickel Phosphorus Copper Study in Corrosive Atmospheric Chamber

E. Yang, Saad K. Doss
and P. Peterson

ELECTROLESS NICKEL PHOSPHOROUS COPPER

Study in Corrosive Atmospheric Chamber

by
E. Yang, Saad K. Doss, and P. Peterson

Abstract

AlMg substrates with an electroless deposited layer of a NiPCu alloy from various plating runs were exposed to a corrosive atmosphere for ten days. The corrosion was monitored by weight gain and optical inspection. Surface roughness, corrosion rates, and film compositions were correlated with plating bath age. The first run has the smoothest surface and the last (30) run has the roughest surface. The roughness has a tendency to increase with the age of the bath. The root mean square roughness of the surface varies from 86 to 276 A^{o}. The arithmetic average roughness varies from 67 to 220 A^{o}; and the peak to valley values run from 475 to 1436 A^{o}. The corrosion rate correlates closely with roughness of the surface. If the effect of the roughness is eliminated, the corrosion rate is almost constant independent of the plating sequence. The corrosion rates in term of weight gain range from 0.23 ug/cm2/hr to 0.28 ug/cm2/hr, which is slightly lower than that of permalloy in the same enviornment.

From the analysis of the corrosion product it was determined that the NiPCu films collect hydrogen chloride most efficiently, sulfur dioxide second, and nitrogen dioxide least.

Introduction

In this study a propriety bath is used to electroless deposit the NiPCu alloy on ground AlMg substrate. The average compositions of electroless plated NiPCu layers are 88% of Ni, 11.3% of P and 0.7% of Cu with no effect from the plating run number. This deposit is amorphous, and hard (with a Knoop hardness of 600 Kg/mm^2 (with a 25g load)) (1), with a highly bright, smooth finish, and defect free. NiPCu films from different runs within the same bath solutions were evaluated for surface roughness, susceptibility to corrosive atmosphere, and composition.

The experiment includes four sections. The first section is surface characterization of NiPCu films, including optical microscopy and roughness measurement. The second section studies accelerating corrosion in atmospheric gas chamber. The third section deals with the analysis of the corrosion products on the substrates. The last part of the experiment contains the composition analysis of the film. The analysis of corrosion products were compared with the composition of the corrosive atmosphere to which they were exposed.

Experimental

The preplating process required the AlMg (AA 5086) ground substrates to be cleaned in an alkaline cleaner, conditioned in an acid deoxidizer, and then double zincated in acid

zincate immersion bath. The plating bath is a proprietary one which operates at 93°C and at a plating rate of 12 um/hr. This experiment used a 400 liter bath. The plating bath was used for a total of 30 runs. Each run consisted of 2.3 square meters surface area. The plating time was 75 minutes per run. There were seven samples selected for this experiment. These samples were taken from runs 1, 5, 10, 16, 20, 25, and 30.

1. Surface Characterization

   Optical microscope was used at magnifications of 100, 200, 500, and 1,000 for visual inspection of the substrates. The roughness of the surface is measured by (Wyko Topo-3D) interferometer for root-mean-square (RMS), average roughness (RA), and peak-to-valley (P-V) in both X and Y directions.

2. Corrosion in the Atmospheric Chamber

   The atmospheric chamber is an accelerating test chamber that controls the desired temperature, relative humidity, various gas concentrations, and air flow (2). The chamber conditions are listed in Table 1.

   Table 1. Conditions of the Environmental Chamber

TEMPERATURE	:	25°C
RELATIVE HUMILITY	:	70% RH
GASES	:	NO2 500 ppb
		SO2 300 ppb
		H2S 40 ppb
		HCl 3 ppb
CARRIER	:	AIR with face velocity 0.5 m/sec

   Seven substrates, one from every fifth plating run, were placed in the chamber. The weights of the substrates were monitored each day and optical micrograph was taken for one substrate to observe the corrosion progress. The substrates were removed from the chamber after ten days.

3. Analysis of Corrosion Products

   The corroded substrates were first extracted with 100 ml of DI water to remove any water soluble corrosion products. The extractant from each substrate was analyzed with a liquid ion chromotographer (Dionex 2020i) (for qualitative and quantitative analysis of inorganic anions). In addition, EDX (energy dispersive x-ray) was employed to identify elements on one substrate after water extraction.

4. Chemical Composition of the Nickel Phosphorous Copper Deposit

   A substrate representative from each run (total of 30 substrates) was cut into small pieces. These pieces were etched in hot 3M NaOH to separate the NiPCu films from the substrates, then weighed (40 to 60 mg), dissolved in 2 ml concentrated HNO_3 acid and volumetrically diluted to 100 ml. A Plasma Spectrometer (Beckman/SMI Spectraspan 5

D.C.) was used to evaluate the Ni, P, and Cu. The analysis indicates that the deposit composition is very consistent throughout the cycle life of the bath.

Results/Discussion

1. Surface Characterization

   Optical microscope photographs of the substrate surfaces from magnification of 500 are shown in Figures 1 through 7.

   From the photographs, the surface finish varies with plating run. The substrate from run 1 has the smoothest surface and the surface from the last run, 30, seems the roughest with large sizes of semispherical NiPCu deposit. In addition, the grinding marks from the substrates are observed on surfaces of as-plated NiPCu deposits.

   The observation on roughness is confirmed by interferometer. The average values of RMS, RA and P-V according to the plating runs are plotted in Figure 8.

   The roughness measurements show a slight increase of roughness with run number. However the last run (30) has double the roughness of the first run.

2. Corrosion in the Atmospheric Chamber

   The photographs of the substrates from run 1 in the corrosion chamber are shown in Figures 9 through 11. These figures show the corrosion progress after 2, 5, and 10 days exposure respectively.

   At the end of first day in the chamber, the corrosion product appeared as submicron droplets on the surface. The droplets grow in size and in number with time in the chamber. The increased number of fringes seen within each drop shows that these drops were increasing in thickness as well as diameter. By the eighth day, solid corrosion products became appearent within these drops.

   Blisters at the edges of the substrate were also seen after 8 days. The mechanism of blistering is due to loss of adhesion between the NiPCu film and the AlMg interface, as the result of corrosion through pin holes in the NiPCu layer (3).

   The weight gains are calculated and plotted as a function of days in the chamber for each substrate in Figure 12. After an initiation period of 2 days, the weight gains increased linearly with exposure in the chamber.

   In general, the amount of corrosion increases with run number. The weight gains per unit area per hour after 10 days in the chamber plotted according to run number are shown in Figure 13. The amount of corrosion correlated better with surface roughness than run number as shown in Figure 8 and Figure 13. For example, run 16 is smoother than run 10, consequently the weight gain of run 16 is less

than run 10. The same applies to runs 20 and 25.

The correlation between corrosion weight gain in the atmospheric chamber and roughness is presented in Figure 14, as weight gain versus roughness. Using a first order approximation to relate corrosion to roughness and factoring the roughness variable out of the data, no corrosion rate dependence on plating run sequence was shown. If the effect of roughness is eliminated, the corrosion rate of NiPCu layers in the chamber is independent of plating run sequence, as shown in Figure 15.

The roughness of the surface contributes to the corrosion rate of the substrate, this can be explained by the microscopic surface area. The rougher the surface, the more surface area is available for corrosion. Therefore, the corrosion rate in term of weight gain is higher for rougher surface. However, the corrosion rate does not depend on the sequence of plating run and the age of the bath if the effect of roughness is removed.

3. Analysis of Corrosion Products

From liquid chromotography, Cl^-, NO_3^{-2}, and SO_4^{-2} were the only anions detected in the water extractions. Figure 16 shows bar charts on molar concentrations of ions. The sulfate products are the highest in concentration, and the percentages of ions in the extracted solutions are presented in Figure 17. The percentages of ions of each substrate are approximately constant, as shown in Table 2 for average ionic percentages and their standard deviations. The sulfate is almost four times of chloride. However, the chamber gas concentration ratio of (SO_2) to (Cl^-) is 100. That is, although the chloride ion has far less concentration in the corrosion chamber, it reacts more aggressively with NiPCu than the Sulfur dioxide. The sticking efficiency of hydrogen chloride on NiPCu is the greatest; sulfur dioxide is more than an order of magnitude lower than chloride and nitrogen dioxide is two orders of magnitude lower than the chloride.

Table 2. Average Ionic Percentage in Extracted Solutions from Corroded Substrates in Mole

ION	AVERAGE%	STANDARD DEV.	% NORMALIZED WITH Cl
Cl	18.04 %	1.98 %	1.00
N03	15.27 %	1.79 %	0.85
S04	66.69 %	3.68 %	3.75

In addition, optical micrographs of substrate surfaces after DI water extraction are shown in Figures 18 and 19. The photographs are also taken from SEM and EDX for the substrate from run 20 after extraction, shown in Figures 20 and 21. Other than Ni and P, only S (sulfur) is detected in EDX analysis. This remaining sulfur is present as water insoluble nickel sulfur com-

pounds. All of the chloride has been removed by the water extraction.

4. Composition Analysis

The chemical composition of runs 1, 5, 10, 16, 20, 25, and 30 are summarized in Figure 22. The anlysis shows a consistent chemical composition of the NiPCu deposit throughout the bath cycle. The average chemical composition is in Table 3.

Table 3. Average Chemical Composition from 30 NiP Runs

ELEMENT	AVERAGE COMP. (WEIGHT %)	STD DEV.
Ni	88.0 %	0.8 %
P	11.3 %	0.7 %
Cu	0.7 %	0.3 %

Summary

The surface roughness of as-plated substrates vary with plating runs. The roughness increases slightly with run number. The roughness of surface can contribute to the rate of corrosion in the corrosion chamber since the rougher surface provides more microscopic area for corrosion. However, the corrosion rate of NiPCu layers in the corrosion chamber does not increase with the age of the plating bath without the effect of roughness. The variation found between the highest and lowest corrosion rates is not enough to be of any concern. The average corrosion rate in terms of weight gain of these NiPCu deposits is 0.26 ug/cm2/hr comparing to that of permalloy, 0.33 ug/cm2/hr.

The analysis of corrosion products indicates that chloride ions, sulfate ions, nitrate ions and H_2O are the critical pollutants. In addition, the chloride is reacting most efficiently with NiPCu since the concentration of Cl^- to SO_2 is only 1 to 100 and the mole composition ratio of corrosion product is 1 to 4. The compositions of NiPCu layers are almost constant through out the lifetime of the bath. The NiPCu layer contains 88% of Ni, 11.3% of P and 0.7% of Cu.

Acknowledge

The authors would like to thank Cheryl White for her assistant on roughness measurement. Leland Chen for his assistant on SEM/EDX, Kay Sommers for her assistant in obtaining the ion chromotergraphy data, and Jerry Sherrad for maintaining the corrosion chamber.

Reference

1. Electroless NiPCu Plating Bath Performance and its Relation to Deposition Parameters, Saad K. Doss, The 172 nd Meeting of the Electrochemical Society, Inc., Honolulu, Hawaii, October 18-23, 1987.

2. Corrosion Mechanism of Thin Film Disk Magnetic Recording Structures, S. K. Doss and G. A. Condas, ASM ISTFA 1986 Int. Symp. for Testing and Failure Analysis, 8618-003, Oct. 1986.

3. Atmospheric Corrosion of Magnetic Film Structures, S. K. Doss and G. A. Condas, Metal. Trans. 18A, 158, Jan. 1987.

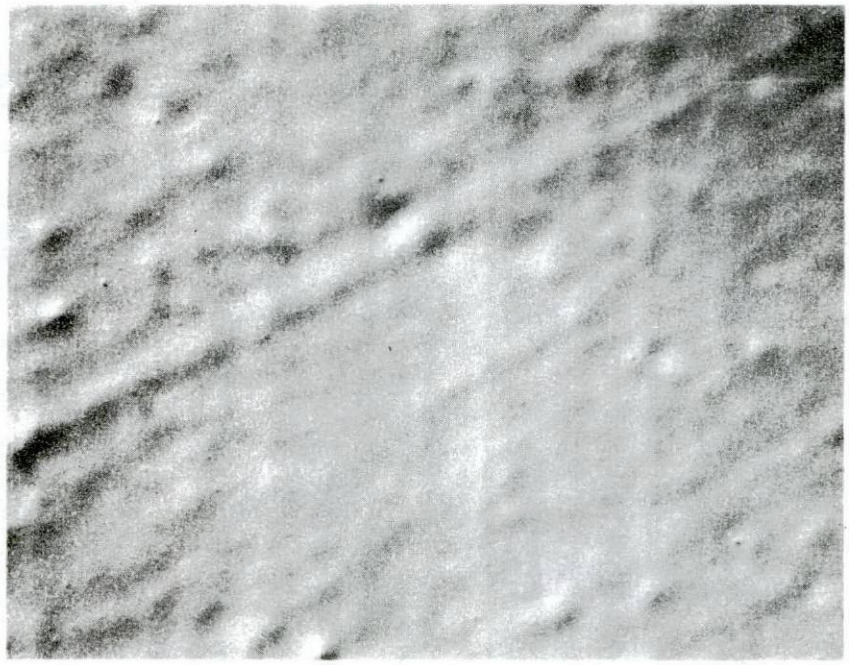

Figure 1. Micrograph of as plated NiPCu on AlMg substrate. Run #1, 500X

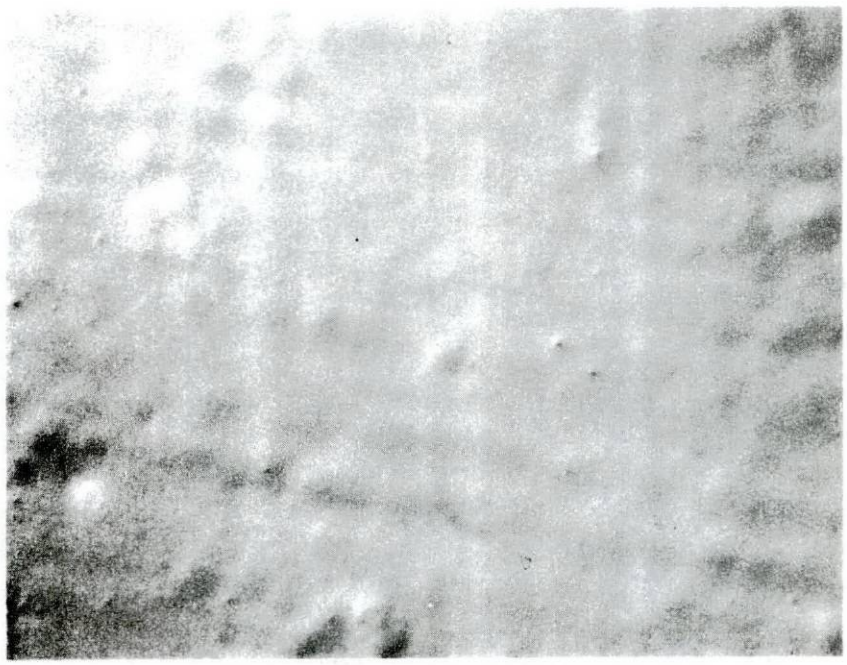

Figure 2. Micrograph of as plated NiPCu on AlMg substrate. Run #5, 500X



Figure 3. Micrograph of as plated NiPCu on AlMg substrate. Run #10, 500X

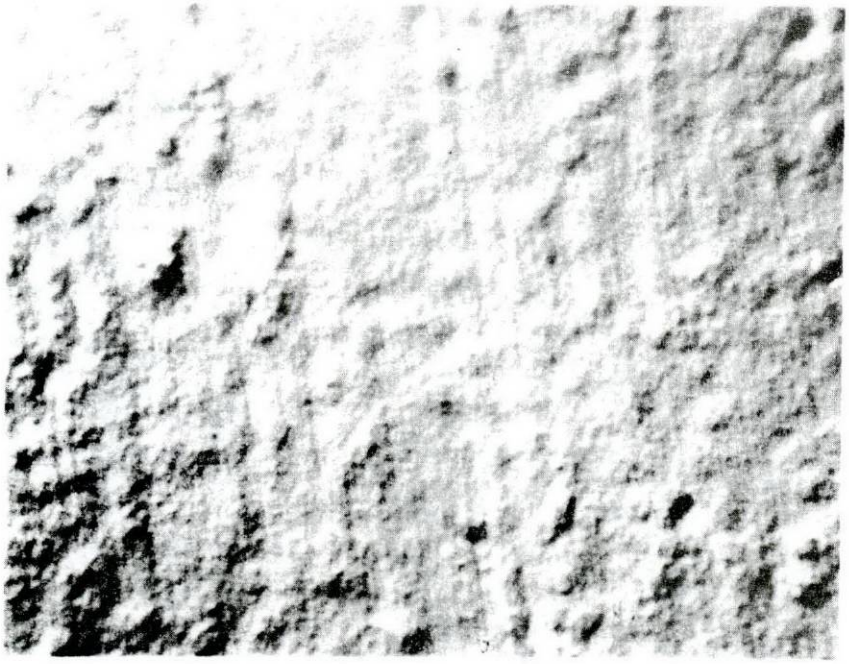

Figure 4. Micrograph of as plated NiPCu on AlMg substrate. Run #15, 500X

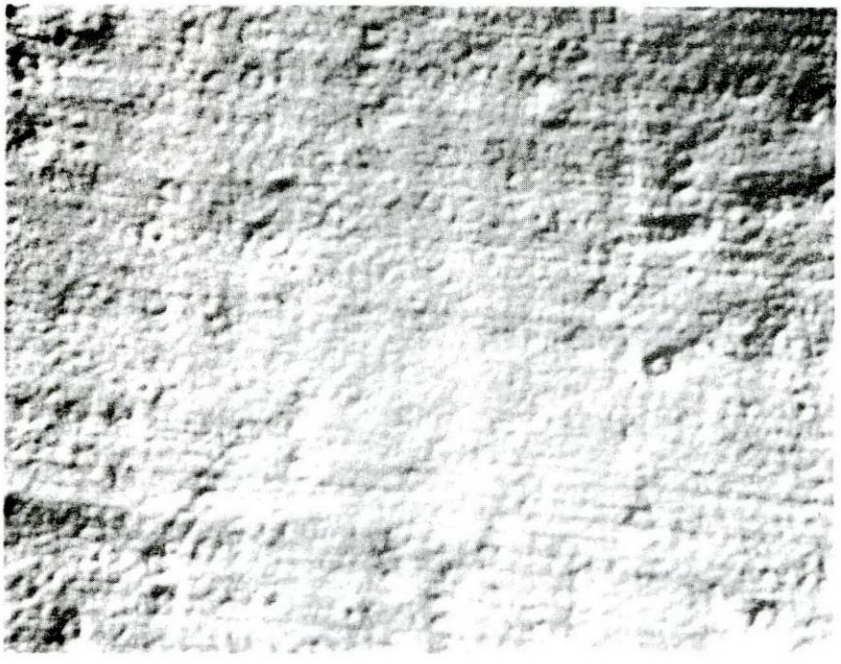

Figure 5. Micrograph of as plated NiPCu on AlMg substrate. Run #20, 500X

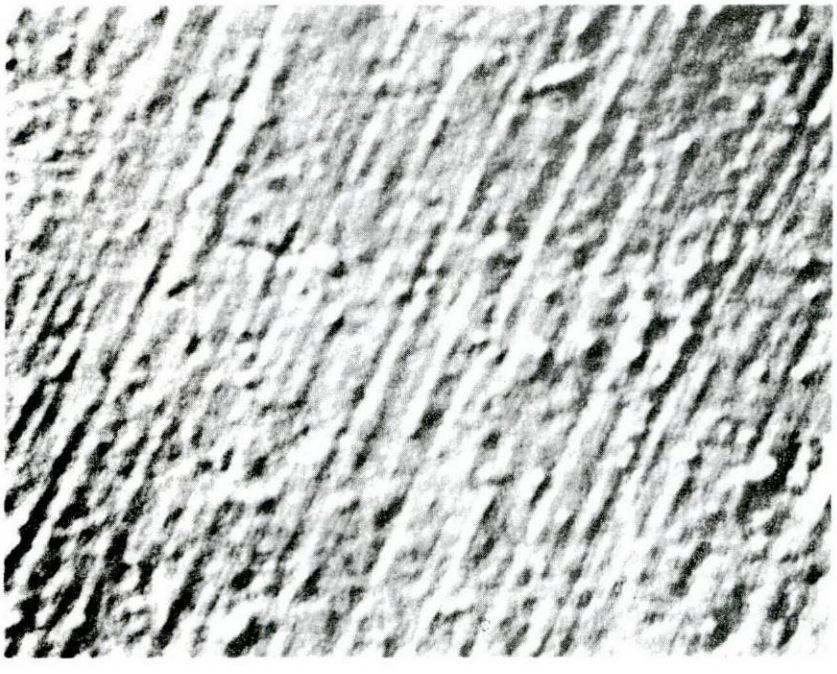

Figure 6. Micrograph of as plated NiPCu on AlMg substrate. Run #25, 500X

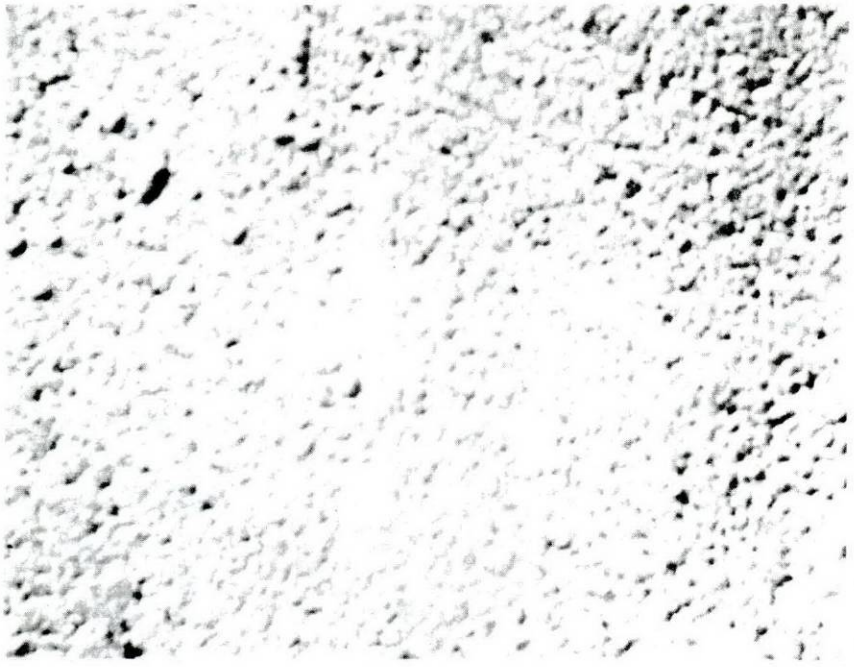

Figure 7. Micrograph of as plated NiPCu on AlMg substrate. Run #30, 500X

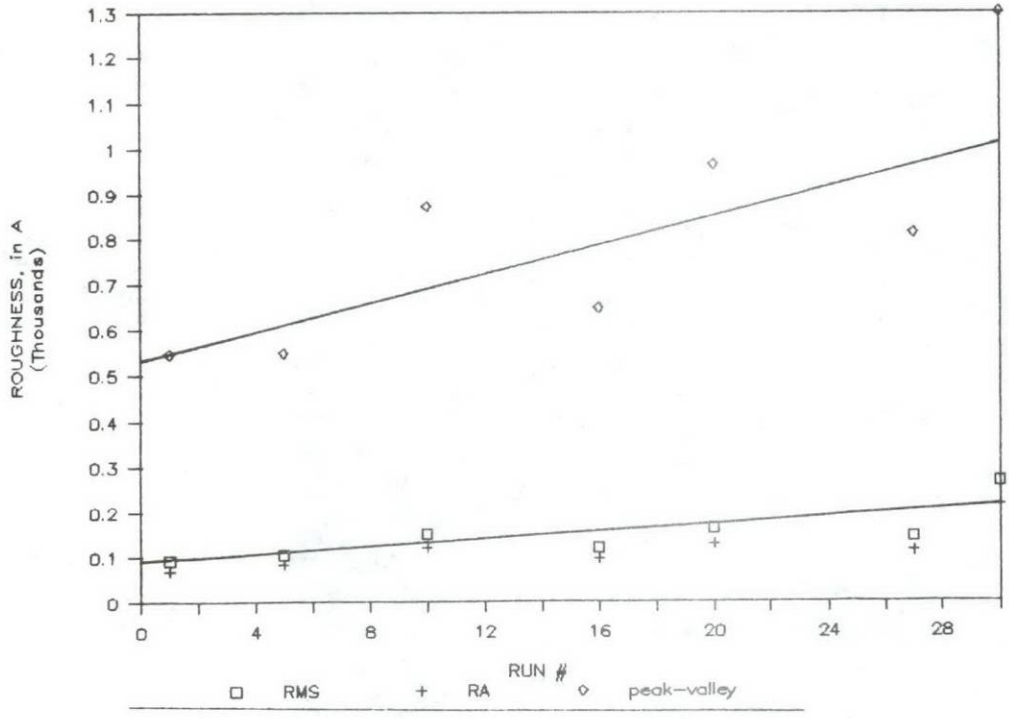

Figure 8. WYKO roughness measurement of NiPCu deposits.

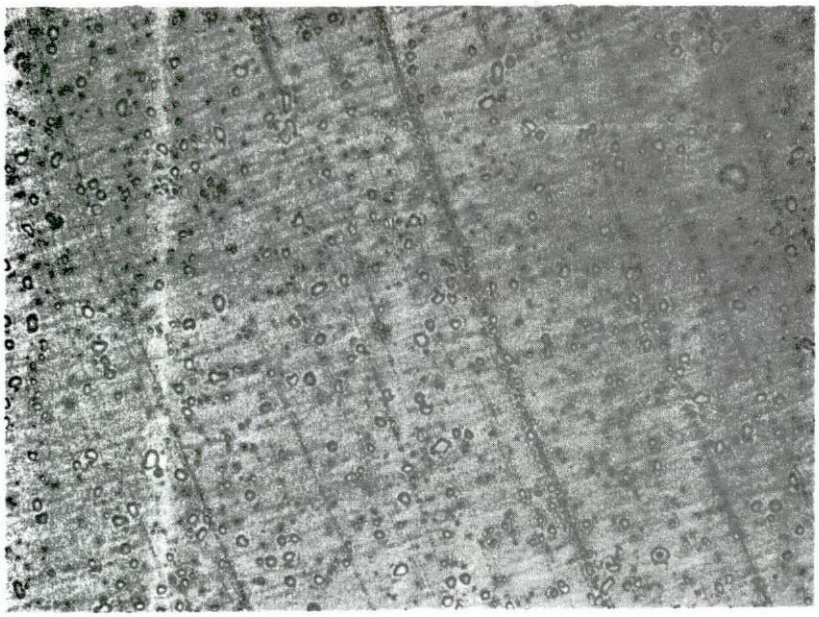

Figure 9. Corrosion progress of NiPCu film after 2 days in the corrosion chamber Run #1, (100X)

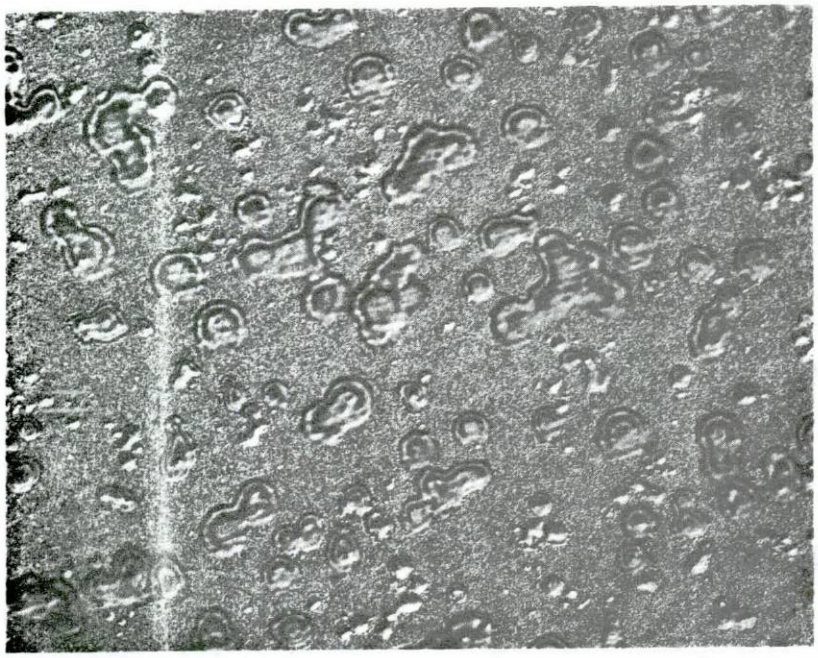

Figure 10. Corrosion progress of NiPCu film after 5 days in the corrosion chamber Run #1, (100X)

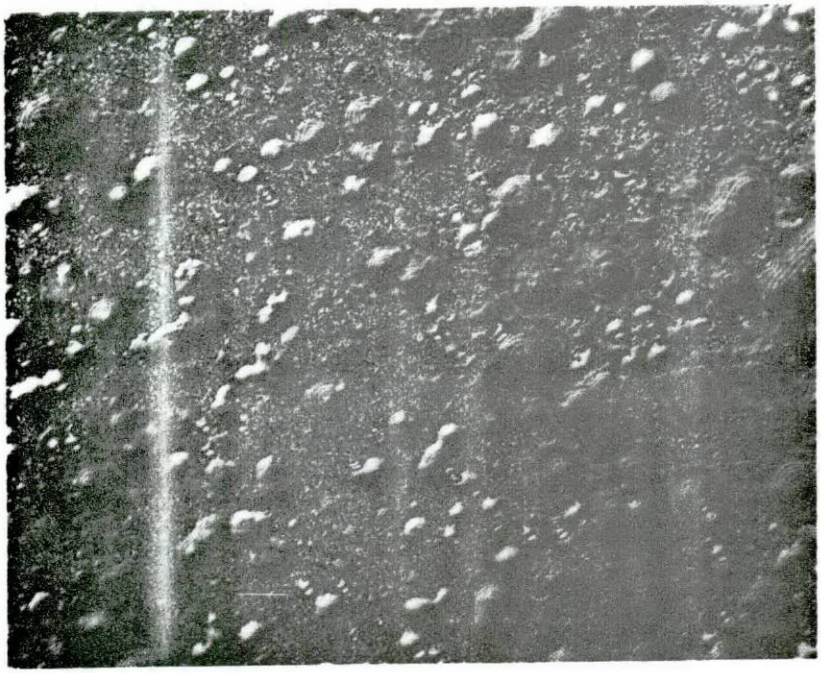

Figure 11. Corrosion progress of NiPCu film after 10 days in the corrosion chamber Run #1, (100X)

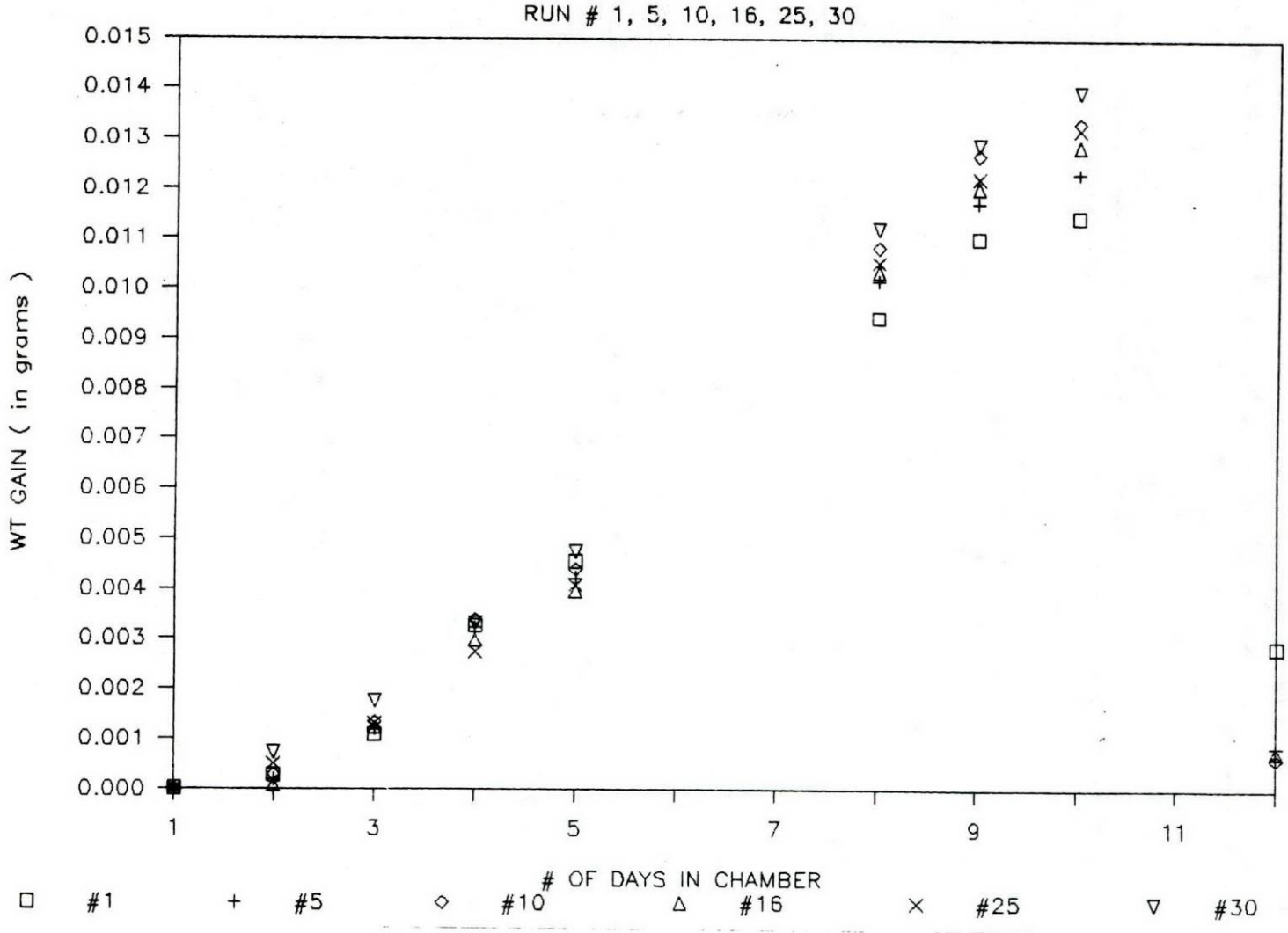

Figure 12. Weight gain in the corrosion chamber.

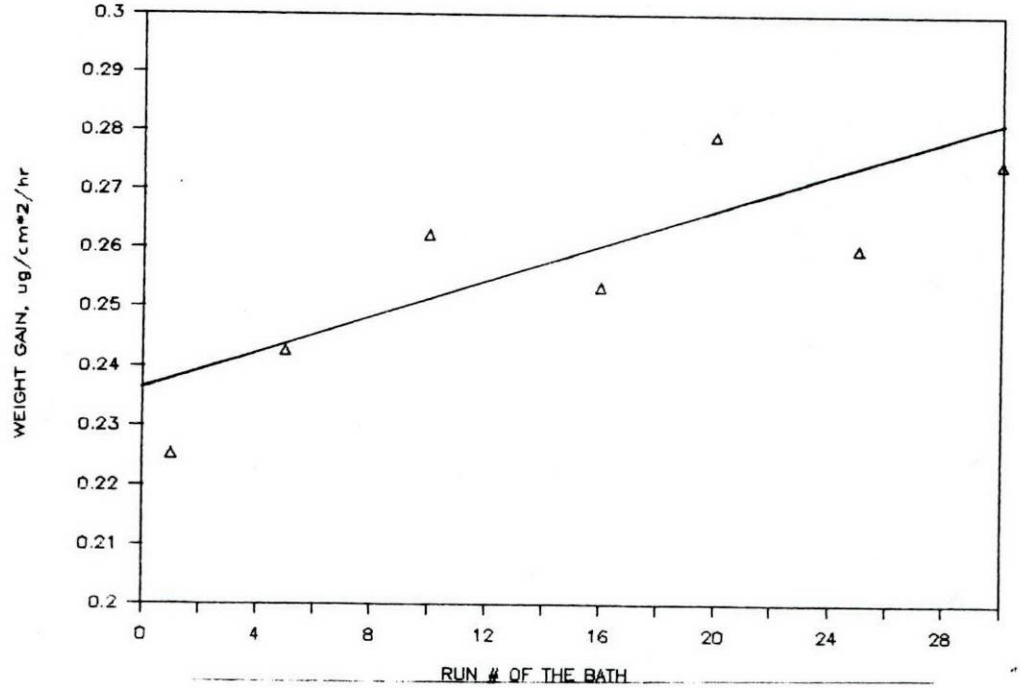

Figure 13. Weight gain measurement (nine days in corrosion chamber).

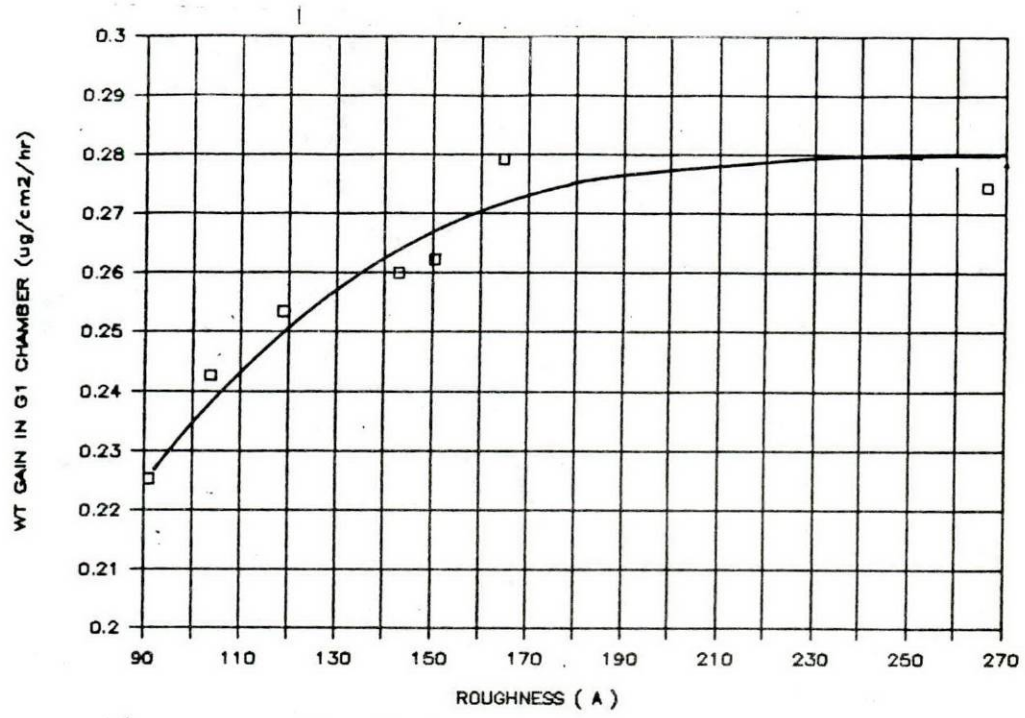

Figure 14. Corrosion rate vs. roughness.

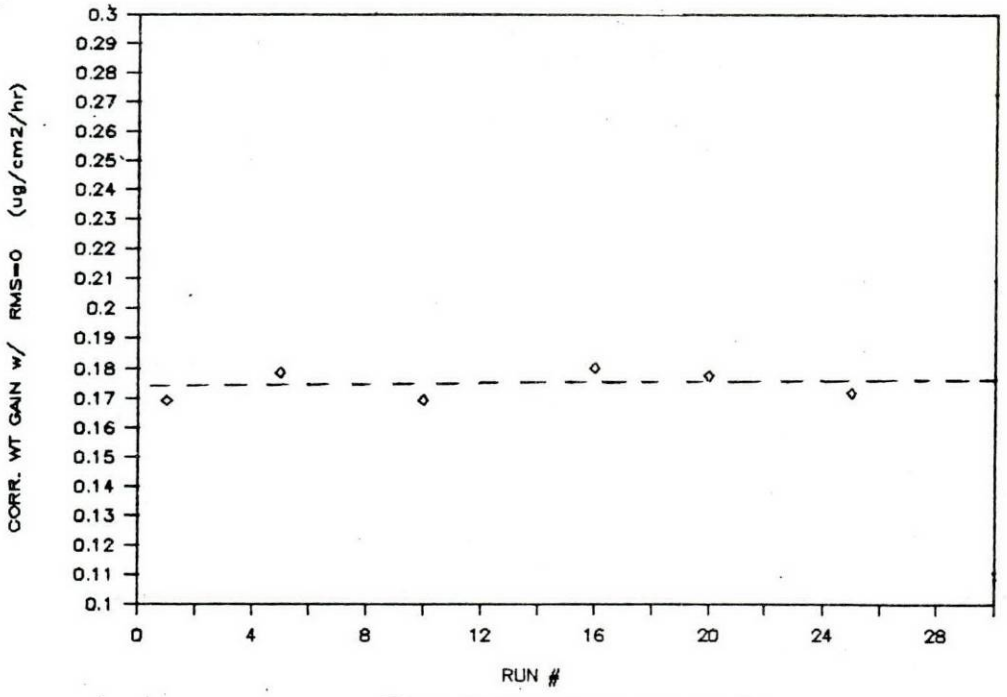

Figure 15. Corrosion rate vs. run No.

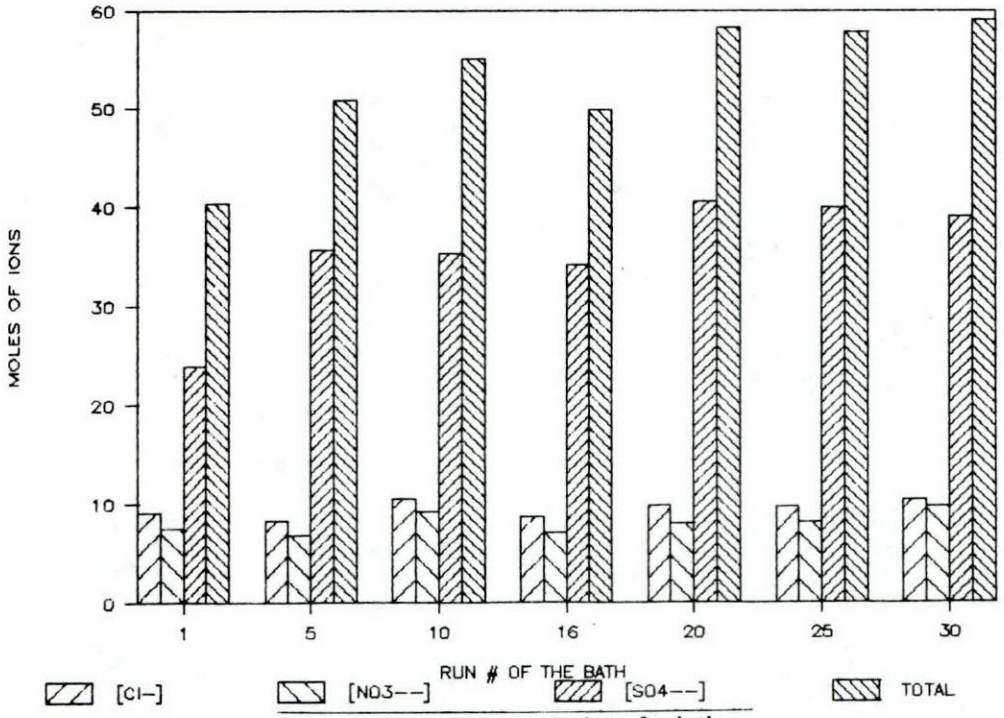

Figure 16. Molar concentration of solution.

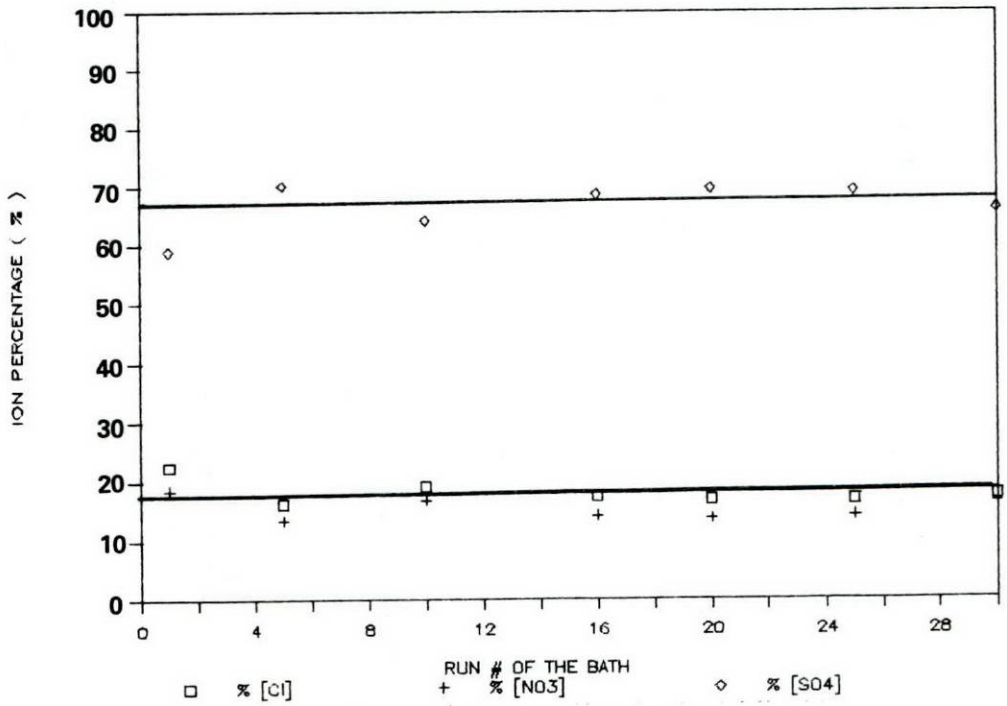

Figure 17. Molar percent of ions in solution.



Figure 18. NiPCu film after water extraction (100X)



Figure 19. NiPCu film after water extraction (1000X)



Figure 20. SEM of NiPCu film after water extraction (2000X)

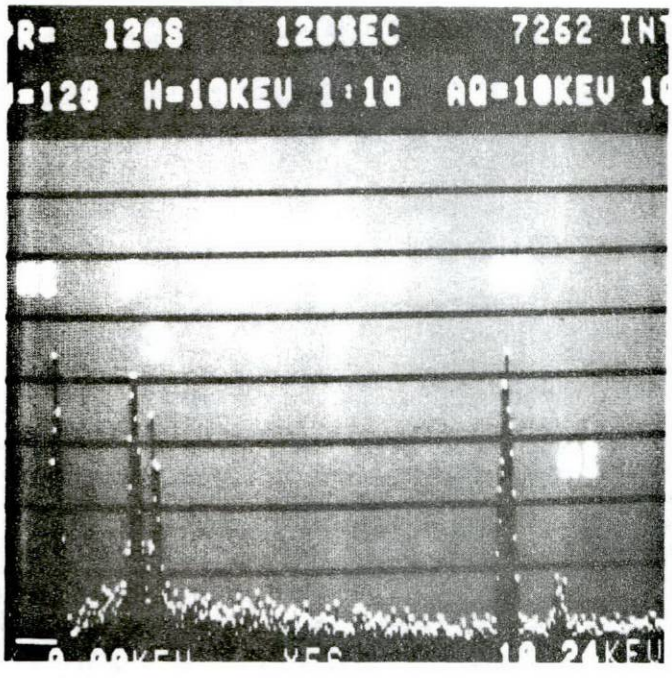

Figure 21. EDX of NiPCu film after water extraction

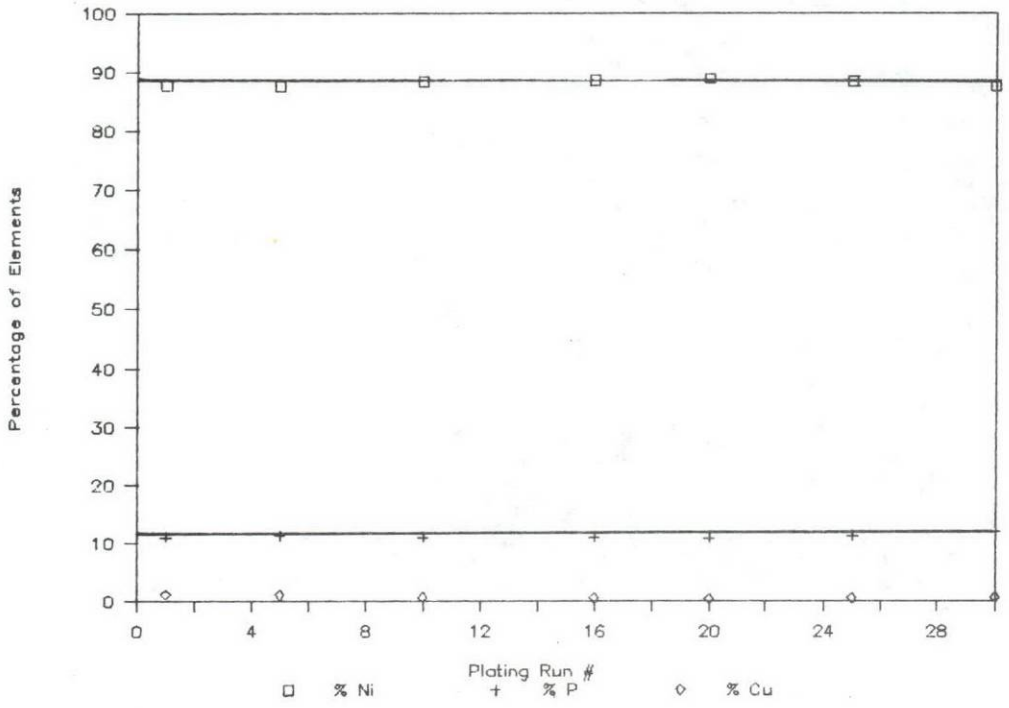

Figure 22 Chemical compositions of NiPCu deposites.

I-2

Electroless Deposition I
Session I

Composite Coatings of Fluorinated Carbon (CFx) In Electroless Nickel Plating Bath

Jung T. Kim
Allied-Signal Inc.
Buffalo Research Laboratory
20 Peabody Street
Buffalo, NY 14210

Composite Coatings of Fluorinated Carbon (CF_x) in Electroless Nickel Plating Bath

Jung T. Kim

Allied-Signal Inc.
Buffalo Research Laboratory
20 Peabody Street
Buffalo,New York 14210

ABSTRACT

Fluorinated carbon (CF_x) and nickel are co[illegible]om an electroless nickel plating bath onto a suitable sol[illegible]g a thin surface layer having low surface energy and good [illegible]CF_x particles with various particle size (from 0.2μm [illegible]e dispersed in aqueous solution containing a nonionic s[illegible]aving HLB number of 10 to 20, optionally including up [illegible]m 20% of cationic surfactant based on the amount of no[illegible]ctant used. The amount of CF_x codeposited in nickel ma[illegible]es with the CF_x concentration in the bath. The process [illegible]ion of Ni/CF_x bath are discussed.

PAPER WITHDRAWN

I-3

Electroless Deposition I
Session I

Corrosion Characteristics of Electroless Nickel Coatings Developed Using Surface Analysis Techniques

Lawrence Salvati, Jr.
Perkin-Elmer Corporation
Edison, NJ

Diane M. Tramontana
Occidental Chemical Corporation
Grand Island, NY

CORROSION CHARACTERISTICS OF ELECTROLESS NICKEL COATINGS DEVELOPED USING SURFACE ANALYSIS TECHNIQUES

Lawrence Salvati, Jr., Perkin-Elmer Corporation, Edison, New Jersey

Diane M. Tramontana, Occidental Chemical Corporation, Grand Island, New York

INTRODUCTION

The effect of phosphorus content on the corrosion behavior of metals and alloys has been studied in various forms.[1-5] Detrimental effects of alloys with phosphorus segregated to grain boundaries include increased susceptibility to intergranular corrosion and stress corrosion cracking. The beneficial effects of phosphorus are mainly observed in amorphous alloys and electroless nickel coatings. The ability of the phosphorus to influence in a positive and negative manner suggests that it can also influence the corrosion performance of the surface layers. J. Flis and D.J. Duquette[1] have shown that increased anodic dissolution and catalytic activity for electroless plating is apparently associated with the deterioration of a passivating oxide film. Electron Spectroscopy for Chemical Analysis (ESCA) studies [6,7,8] have shown evidence of P^5 species (as phosphates) in the surface layers of phosphorus containing alloys. It has been further suggested, that the appearance of these phosphates significantly contributes to the corrosion protection of the surface layer [1,6,7,8].

Recent corrosion studies [9,10] in chemical process environments have questioned the theory that higher phosphorus contents always enhance the corrosion protection of electroless nickel (EN) alloys. R.P. Tracy et al.[9] demonstrated that lower phosphorus containing alloys (1-2% phosphorus) have superior resistance to corrosion in several chemical process environments (Table 1). The corrosion performance of low phosphorus electroless nickel alloys is especially superior to high phosphorus alloys in sodium hydroxide environments (Table 1). This corrosion behavior of the low phosphorus electroless nickel coating indicates differences in surface film structure and components.

In the present study, Electron Spectroscopy for Chemical Analysis (ESCA or XPS) and Auger Electron Spectroscopy (AES or SAM) were used to characterize a series of Electroless Nickel (EN) coatings. The EN samples investigated included

as-plated, after heat treatment and after corrosion testing in several industrial process environments. In all of these cases, the EN coatings were prepared with varying amounts of phosphorus. The corrosion tested EN materials were the same samples reported on by Tracy et al.

The primary emphasis of this investigation was directed at characterizing the surface composition of as-plated EN coatings. The principle goal of this study was to determine the effects of phosphorus content on the surface chemistry and ultimately the corrosion properties of these materials. Based on the ESCA and angle dependent ESCA (ADESCA) results presented in this report, a correlation between the surface chemistry and phosphorus concentration of the plating bath was clearly indicated. Preliminary ESCA results collected for the corrosion tested samples further suggested that the as-plated surface composition influenced the corrosion properties of the EN coating. In addition, this report will also present data obtained for heat treated EN materials. This data showed that the surface chemistry and composition of the heat treated EN coatings was significantly different from that of the corresponding as-plated material.

EXPERIMENTAL PROCEDURES:

Three electroless nickel coatings were evaluated: low phosphorus (1-2%), medium phosphorus (6-8%), and high phosphorus (10-11%) as expressed in weight percent. In the text, these materials will be referred to by the designations LP, MP, and HP. All three coatings were deposited at a thickness of 50-65 microns. ASTM G-31, "Laboratory Immersion Corrosion Testing of Metals" was used to test the panels. Mild steel (AISI 1010) panels were cleaned using the following cycle: vapor degrease, hot alkaline soak (85^0C), water (DI) rinse, electroactivation with periodic reverse, water rinse, plated, water rinse, and air dried. Only those panels with a negative ferroxyl test were used in the testing program. The surface area was measured, using a digital caliper (=0.01 cm), and recorded. The details of the actual immersion data including the particulars of each chemical environment are presented by R.P. Tracy et al. in reference 9.

The ESCA and ADESCA measurements were obtained using a Perkin Elmer Model 5000 LS Spectrometer. A Mg anode (Mg$k\alpha$ =1253.6eV) run at 400 watts (15kV and 27mA) was employed as the primary x-ray source. The vacuum inside the main analytical chamber was typically better than $5x10^{-9}$ Torr. The binding energy positions of the photoelectron lines were determined by referencing to the C1s line at 284.6eV. All

instrument operations, data acquisitions and data massage routines were accomplished using a Perkin Elmer Version 2.0 ESCA software package.

The AES results were obtained on a Perkin Elmer Model 660 SAM system. This system utilizes a LaB_6 filament with a minimum beam diameter of 250Å. The beam voltage was variable between 1 and 30keV. The results presented here were obtained at a beam voltage of 5keV and beam current of approximately 1 μA. The base vacuum inside the main analytical chamber was < $1x10^{-9}$ Torr. Sputter depth profiling was accomplished using a Model 06-650 duoplasmatron ion gun. The primary beam voltage in the ion gun was 4 keV with ^{40}Ar as the sputtering gas. The sputter rate at these conditions was calculated to be 65Å/min for SiO_2/Si.

RESULTS AND DISCUSSION

As Plated EN Coatings

The initial section of this discussion presents the ESCA and ADESCA results obtained for the as-plated LP, MP, and HP EN materials. ESCA survey spectra collected for the as-plated EN materials indicated the presence of Ni, O, C, and P. The Ni and P peaks were expected, since the EN process involves the co-deposition of both of these elements. The presence of oxygen was most likely due to surface oxidation and adsorption of H_2O, while atmospheric contamination was the probable source of the C peak. High resolution spectra were obtained for each of these elements. This data was used to more closely evaluate the chemical and quantitative composition of the EN surfaces.

High resolution spectra acquired for the Ni2p region were similar for all of the as-plated EN materials investigated. An example of the Ni2p spectrum obtained for the as-plated surfaces is illustrated in Figure 1. The spectra consisted of six peaks (labeled I-IV and S). The spectra appeared complex, but the interpretation was straightforward. Due to the inherent energy separation of the $2p_{3/2}$ - $2p_{1/2}$ atomic levels in the nickel atom, the Ni2p photoelectron spectrum characteristically exhibits two peaks. The peak separation exhibited by the nickel spin orbit doublet ($Ni2p_{3/2,1/2}$) is a direct reflection of the atomic energy level difference and typically falls within the range of 17-18eV. The exact energy difference is characteristic of the particular nickel species present. Based on this information, it was concluded that the Ni2p spectra (Figure 1) reflected the presence of two distinct nickel species resulting in two sets of Ni2p

doublets. The two low energy peaks (I and III) were identified as $Ni2p_{3/2}$ lines, while the peaks centered around 872 eV (II and IV) were the corresponding $Ni2p_{1/2}$ lines. The additional lines designated S represented shake up satellite lines.

Identification of the nickel species was based on the measured binding energy positions of the $Ni2p_{3/2}$ lines (peaks I and III). The binding energy of peak I (Figure 1) was determined to be approximately 852eV which compared with the literature value for metallic nickel [15]. The position of line III was approximately 856.5eV which matched the reference value for $Ni(OH)_2$ [15-16]. It is beyond the scope of this report to discuss the origin of the shake up lines in any detail. For the purposes of this discussion, it is sufficient to state that the peak shape and position of the shake up lines (S) correlated closely with published reference spectra for $Ni(OH)_2$ [16]. This confirmed the presence of $Ni(OH)_2$ on the as-plated EN surfaces.

High resolution ESCA spectra obtained for the P2p region also supplied valuable information concerning the chemistry and composition of the as-plated EN materials. The phosphorus spectra exhibited two peaks for all of the as-plated EN samples. The binding energies of these peaks were measured at approximately 129eV and 133eV. Unlike the Ni2p region, the spin orbit splitting for the $P2p_{3/2,1/2}$ lines is approximately 1.0eV [18] and is not easily resolved by ESCA. Based on this data, it was concluded that two distinct phosphorus species were present. The binding energy values measured for these peaks suggested the presence of free phosphorus plus a PO_4^{-3} type species. The peak at 129eV was characteristic of free phosphorus. The peak at a binding energy position of ~133eV was characteristic of a PO_4^{-3} species [15].

The Ni2p and P2p data discussed above indicated the presence of a thin (<100Å) "passive" oxide layer comprised of $Ni(OH)_2$ and PO_4^{-3} on the as-plated EN surfaces. In the region below this oxide layer, the data suggested that the coating consisted of nickel metal and free phosphorus. To formulate a better understanding of the surface composition, a series of ADESCA measurements were obtained which provided a non-destructive depth profile of the coating surface. Figures 2 and 3 illustrate representative ADESCA spectra collected for the as-plated EN coatings, while the corresponding atomic concentration (AC) results are listed in Tables 2 and 3.

Figure 2 illustrates the $Ni2p_{3/2,1/2}$ spectra collected for the as-plated a) LP, b) MP, and c) HP coatings at a 90^0 take off angle. These results implied that the depth of the

oxide overlayer was dependent on the phosphorus content of the coating. This observation was based on the fact that the relative nickel metal/$Ni(OH)_2$ peak heights varied significantly for the different EN materials. In the LP spectrum (Figure 2a), the nickel metal peak was most intense, while for the HP sample (Figure 2c), the predominant nickel species was $Ni(OH)_2$. It was apparent from these spectra that the relative Ni/$Ni(OH)_2$ peak height ratio decreased systematically as the phosphorus content of the coating was incremented. This trend indicated that the oxide ($Ni(OH)_2$) overlayer thickness was dependent on the phosphorus content of the coating and/or plating bath.

The P2p ESCA spectra for as-plated a) LP, b) MP, and c) HP coatings at 90^0 are presented in Figure 3. As with the nickel results (Figure 2), the phosphorus spectra also demonstrated differences in chemical composition as a function of the phosphorus content in the deposit. In this case, the spectra showed an increase in the P/PO_4 peak height ratio as the phosphorus content was incremented. This behavior was opposed to that demonstrated by the nickel spectra (Figure 2). Whereas the HP EN deposit was characterized to have the thickest oxide, the P/PO_4 ratio for this sample was significantly greater than that determined for the LP sample.

The ADESCA spectra shown in Figures 4 and 5 further supported the presence of a thin $Ni(OH)_2$ overlayer. The Ni2p spectra illustrated in Figure 4 demonstrated the classic behavior characteristic of a uniform overlayer. In other words, the oxide peak dominates the surface (15^0) spectrum, but as the sampling depth is increased (higher θ), the peak due to nickel metal grows relative to the oxide peak. The explanation for the phosphorus ADESCA data was not as straightforward. In this case, the spectra did exhibit the expected behavior with the relative contribution of the free phosphorus peak increasing as the take off angle was incremented from 15^0 to 90^0. It was also evident from the spectra that the phosphorus concentration detected by ESCA was greater as the sampling depth was increased.

Atomic concentration values calculated from the ADESCA spectra provided a semi-quantitative depth profile of the surface composition. These values are listed in Tables 2 and 3. In addition, P/Ni ratios have also been tabulated to facilitate direct sample to sample comparisons. The figures in Table 2 represent the AC values obtained for as-plated LP, MP, and HP coatings at angles of 30^0 and 90^0. Table 3 includes a comprehensive AC data set for LP and HP coatings at angles of 15^0, 30^0, 45^0, and 90^0.

It was obvious from the data (Table 2), that the distribution of phosphorus within the surface region varied as a function of the bulk phosphorus concentration. In addition, the data further indicated a non-uniform distribution of phosphorus within each individual material. For example, Table 2 shows that the P/Ni ratios declined in the order LP > MP > HP at a take off angle of 30^0, while at 90^0 the opposite behavior was observed (i.e. LP < MP < HP). The ADESCA results presented in Table 3 show that the P/Ni ratio drops steadily as a function of take off angle for the LP coating. Conversely, the HP results showed an increase in the ratio as the sampling depth was expanded.

The combined results obtained for the as-plated EN coatings provided a comprehensive picture of the surface composition. The data clearly showed the existence of a thin oxide overlayer composed of predominantly $Ni(OH)_2$. It was further demonstrated that the thickness of this oxide layer varied as a function of the phosphorus content in the deposit. The LP material was determined to have the thinnest oxide and the HP material the thickest. In all cases, the thickness of the oxide was less than the sampling depth of the ESCA technique (20-100Å).

It was also apparent from this investigation that phosphorus was depleted in the oxide region. This conclusion was based on the observed behavior of the P/Ni ratios presented in Tables 2 and 3. The LP material was characterized to have the thinnest oxide, yet this same material exhibited the highest surface (15^0) P/Ni ratio. At the same time, the P/Ni ratio calculated for the 90^0 data yielded the lowest value. These results suggested that the phosphorus was predominantly associated with the metallic nickel. The PO_4^{-3} species detected was most likely located at the metal/oxide interface.

Heat Treated EN Coatings

ESCA and AES data was obtained for LP and HP EN coatings before and after heat treatment. The Ni $2p_{3/2,1/2}$ data for a HP sample a) as-plated and b) after heat treatment is pictured in Figure 6. The heat treated material produced a spectrum that differed significantly from the as-plated coatings. Only one form of nickel was evident in this spectrum, which based on the peak position and peak shape was identified as NiO [15]. The fact that a nickel metal peak was not observed suggested that the oxide overlayer was thicker than the sampling depth of ESCA (~ 100Å). This was confirmed by AES sputter depth profiling. Similar results were also obtained for the heat treated LP material.

Figure 7 illustrates the corresponding P2p spectra obtained for the a) as-plated and b) heat treated HP sample. The P2p spectrum of the as-plated sample compared closely with the spectra previously presented in Figure 3. For the heat treated HP EN coating, the spectrum (Figure 7b) exhibited two peaks at a binding energy of approximately 139eV and 144eV. The measured binding energy positions of these peaks were too high to be representative of a phosphorus species. After careful consideration, it was concluded that this spectrum was characteristic of the $Pb4f_{7/2,5/2}$ spin orbit doublet. The source of lead was not definitely known, but lead ions are often used as stabilizers in EN plating baths [14]. The P2p spectra acquired for the LP sample were similar to those shown in Figure 7.

Auger sputter depth profiling was employed to determine the oxide thickness and phosphorus distribution of both the as-plated and heat treated coatings. The resultant profiles obtained for the HP EN sample a) as-plated and b) after heat treatment are presented in Figure 8. This data showed that the depth of the oxide layer was much greater for the heat treated coating than for the as-plated sample. In the profile for the as-plated sample, the oxygen level dropped to near 0 atomic percent within the first minute of sputtering which indicated that the oxide layer was less than 100Å. This agreed with the conclusions determined from the ADESCA data. The profile showed the phosphorus level increasing from ~10% to a steady state value of ~30% in the bulk. As a comparison, the results collected for the LP sample indicated an initial phosphorus concentration of ~12% and a steady state value near 18 atom percent. In both instances, the concentration values quoted were based on the standard Auger sensitivity values.

The corresponding sputter depth profile of the heat treated coating is shown in Figure 8b. Based on this data, the oxide thickness was estimated to be 150-200Å. The oxygen level remained equal to the nickel concentration of ~45% for the first 2-3 minutes of the profile. In this same region, no appreciable concentration of phosphorus was detected. At approximately 3.5 minutes, the oxygen level dropped sharply and the phosphorus level rose rapidly above 37% before declining to an equilibrium value of approximately 30%. This bulk phosphorus concentration compared closely with the results of the as-plated coating (Figure 8a).

These results clearly demonstrated that the heat treatment process significantly affects the surface chemistry and composition of EN coatings. The data showed that heat treatment produces a relatively thick NiO layer which was depleted of phosphorus. The oxide layer was estimated to be

150-200Å, relative to the as-plated samples which were found to have much thinner (20-100Å) oxides. The data further indicated that the growth of the oxide occurred through a diffusion process. This process formed the NiO layer, while the phosphorus remained in the "bulk". This growth process was suggested based on the enhanced phosphorus levels apparent in the profile at the oxide/metal interface.

Corrosion Tested EN Coatings

The final segment of this investigation involved the characterization of the LP, MP, and HP EN coatings after 60 days of exposure to one of the industrial process environments listed in Table 1. The samples analyzed were the same materials used by Tracy [9] to measure corrosion rates. ESCA spectra were recorded for all of the samples listed (Table 1). At this point, only the preliminary results of the surface characterization study will be discussed. Data for EN coatings exposed to orthochlorobenzyl chloride (OCBC), benzotrichloride (BOC), phosphoric acid (H_3PO_4), and 73% caustic soda (NaOH/NaCl) will be presented. The results obtained for the corrosion tested samples were difficult to interpret due to the complexity of the test environments employed.

Table 4 lists typical ESCA AC results obtained for the EN coatings listed above. The results presented show that some corroaents had a significant effect on the surface composition of the EN coatings, while for other environments the surface composition was relatively unchanged. The changes in surface composition were most evident from the P/Ni ratios. The samples tested in an OCBC environment exhibited P/Ni ratios very similar to those measured for the as-plated materials. Materials exposed to H_3PO_4 and NaOH/NaCl environments showed a significant depletion in the surface phosphorus concentration.

Changes resulting from the corrosion testing were also evident in the high resolution Ni2p and P2p ESCA spectra recorded. Figures 9 and 10 illustrate several examples of the Ni2p spectra obtained for the tested EN coatings. Figure 9 includes the spectra acquired for HP coatings exposed to a)OCBC, b)BOC and c)H_3PO_4 environments. The spectrum of the sample tested in OCBC (Figure 9a) indicated the presence of nickel metal and $Ni(OH)_2$. This compared closely with the composition of the as-plated surface. Conversely, only $Ni(OH)_2$ was detected on the sample tested in H_3PO_4 suggesting the presence of an enhanced oxide overlayer.

The results recorded for the LP materials shown in Figure 10 appeared similar to the HP results (Figure 9). There were, however, some notable differences. For example, the spectrum of the OCBC exposed sample indicated the presence of a thicker oxide layer than that for the corrosion tested HP sample (Figure 9a). In comparison, the oxide layer was determined to be thinner for the LP coating as-plated. Differences were also observed for the EN coatings tested in H_3PO_4. Comparing the corrosion tested LP and HP materials suggested that oxide layer was greater for the HP coating.

The ESCA results collected for the corrosion tested samples implied that the surface composition of the as-plated coating has a direct affect on the corrosion properties of the EN surface. More importantly, the results indicate that the as-plated surface interacts differently for each type of corrodent tested. For some corrodents, the LP coating yielded the best results, while for other environments it was the HP or MP coatings that exhibited the superior corrosion protection.

SUMMARY

The results of this investigation clearly demonstrated that the surface composition of EN deposits were dependent on the phosphorus content of the coating. This study involved EN deposits with three different phosphorus levels. For each of these coatings, the surface composition was shown to be similar in some respects and different in others. All three of the EN materials characterized were found to have a thin (<100Å) overlayer of $Ni(OH)_2$. The bulk species was nickel metal. Phosphorus was determined to be present in two forms; phosphate and free phosphorus. However, the distribution of these phosphorus species within the surface region was found to vary with the phosphorus content of the coating.

These differences were most readily apparent from the ADESCA results presented in Figures 4-5 and Tables 2-3. It was determined that the depth of the oxide ($Ni(OH)_2$) overlayer varied in the order LP < MP < HP. These results also suggested that phosphorus was depleted in the oxide layer. The PO_4^{-3} species detected was most likely located at the metal/oxide interface. The free phosphorus was associated with the nickel metal in the bulk of the coating. These conclusions were based on the observed differences in the P/Ni ratios (Table 3). For the surface (15^0 and 30^0) measurements, the P/Ni ratio was highest for LP and lowest for HP. At a take off angle of 90^0, the P/Ni ratios fell in the expected order; HP > MP > LP.

Heat treatment was shown to produce a thick oxide on the EN surface. This oxide was identified as NiO and the thickness was estimated to be approximately 200Å. As with the oxide present on the as-plated samples, no phosphorus was detected in the oxide formed during the heat treatment process. Two types of EN, low phosphorus and high phosphorus, produced similar results with the exception of the bulk phosphorus level measured. The AES sputter depth profile results indicated that the oxide was formed by nickel diffusion, which resulted in a pile up of phosphorus at the metal/oxide interface.

The final segment of this investigation involved the surface characterization of LP, MP, and HP EN coatings in a series of industrial process environments. The results obtained for these materials indicated a strong correlation between the composition of the as-plated surface and the resultant corrosion protection of the coating. The interpretation of the data, however, was unclear due to the complexity of the chemicals used in the corrosion testing experiments. It seems evident that a more controlled set of corrosion experiments could provide a better understanding of the affect of surface composition on corrosion properties of EN materials.

REFERENCES:

1. J. Flis and D.J. Duquette, Corrosion, Vol. 41, No. 12, p. 700-706, Dec. 1985.

2. J.S. Armijo, Corrosion, Vol. 24, No. 1, p. 24, 1968.

3. A. Joshi, D.F. Stein, Corrosion, Vol. 28, No. 9, p. 321, 1972.

4. C.L. Briant, Corrosion, Vol. 36, No. 9, p. 497, 1980.

5. C.L. Briant, Corrosion, Vol. 38, No. 4, p. 230, 1982.

6. K. Hashimoto, T.J. Masumoto, Non-Cryst. Solids, Vol. 28, p. 403, 1978.

7. K. Hashimoto, Passivity of Metals and Semiconductors, M. Fremont, Ed., Elsevier, Amsterdam, p. 235, 1983.

8. P. Cadet, M. Keddam, H. Takenouti, 4th Int. Conf Rapidly Quenched Metals, Sendai, p. 1447, 1981.

9. R.P. Tracy, J.F. Colaruotolo, A. Misercola, B.R. Chuba, Materials Performance, p. 21-29, August 1986.

10. R.P. Tracy and B.R. Chuba, Corrosion 87, Paper No. 462, March 9-13, 1987.

11. C.J. Powell, Amer. Lab., Vol. 10, No. 4, p. 17, 1978.

12. D.M. Hercules and S.H. Hercules, J. Chem. Ed., Vol. 61, No. 6, p. 483, 1987.

13. C.J. Powell, Scanning Electron Microscopy, 1984 IV, p. 1649, 1984.

14. K. Parker, Plating and Surface Finishing, p. 60-65, February, 1987.

15. W.M. Riggs, L.E. Davis, J.F. Moulder, and G.E. Muilenberg (ed.), Handbook of X-ray Photoelectron Spectroscopy, Perkin Elmer Corp., MN, 1979.

16. N.S. M^{C}Intyre and M.G. Cook, Anal. Chem., Vol. 47, No. 13, p. 2208, 1975.

17. N.S. M^{C}Intyre, T.E. Rummy, M.G. Cook, and D. Owen, J. Electrchem. Soc., Vol 123, p. 1165, 1976.

18. T.A. Carlson, Photoelectron and Auger Spectroscopy, Plenum Press, New York, 1975.

COMPARISON OF EN CORROSION RATES VS. OTHER COMMONLY USED MATERIAL IN CHEMICAL PROCESS ENVIRONMENTS

All Corrosion Rate in μm/yr., 60 Days Exposure at 40°C ∓2°C

		EN Coatings				
Corrodent*	Nickel 200	Low Phosphorus (1-2%)	Medium Phosphorus (6-8%)	High Phosphorus (10-12%)	Mild Steel	AISI 316 SS
Thionyl Chloride	7.0	900.0	1.8	2.5	200.0	5.1
Orthochlorobenzyl Chloride (Crude)	12.7	3.8	7.4	7.1	NA	25.0
Orthochlorobenzyl Chloride	12.7	5.3	13.5	9.4	NA	25.0
Phosphoric Acid	10.0	900.0	193.0	19.3	1270.0	2.5
73% Caustic Soda**	5.1	2.3	7.4	F	1448.0	332.7
Phosphorus Oxychloride	10.0	28.4	1.5	2.5	100.0	18.8
Benzotrichloride	5.1	2.5	5.6	6.1	9.0	5.1
Benzoyl chloride	5.1	1.0	0.8	0.5	8.6	5.1

*Corrodents used in this study were of final product grade except where noted

NA = No data available
** = 100 Day Exposure
F = Failed

TABLE 2

ADESCA RESULTS FOR AS PLATED EN COATINGS

	Ni	O	C	P	P/Ni
$\Theta = 30^\circ$					
LP	1.44	27.59	68.64	2.32	1.61
MP	1.92	23.89	71.79	2.40	1.25
HP	1.66	20.93	75.63	1.78	1.07
$\Theta = 90^\circ$					
LP	5.92	37.01	53.23	3.84	0.65
MP	5.84	31.24	54.06	8.87	1.52
HP	4.06	29.26	59.65	7.03	1.73

TABLE 3

ADESCA RESULTS FOR LP & HP EN COATINGS

	Ni	O	C	P	P/Ni
Low Phosphorus					
15°	0.89	19.14	78.51	1.46	1.64
30°	1.44	27.59	68.64	2.32	1.61
45°	2.15	32.27	62.83	2.75	1.28
90°	5.92	37.01	53.23	3.84	0.65
High Phosphorus					
15°	0.96	15.07	83.13	0.83	0.86
30°	1.66	20.93	75.63	1.78	1.07
45°	2.25	25.39	68.99	3.37	1.50
90°	4.06	29.26	59.65	7.03	1.73

TABLE 4

ESCA RESULTS FOR CORROSION TESTED EN COATINGS

Corrodent		Ni	O	C	P	P/Ni
OCBC-F.P.	HP	11.3	38.4	42.7	7.4	0.66
	MP	12.0	39.6	40.9	7.6	0.63
	LP	6.8	30.1	58.4	4.7	0.69
OCBC-C	HP	8.1	31.9	51.1	8.5	1.1
	MP	3.6	27.8	61.4	6.1	1.7
	LP	8.5	27.6	56.6	5.1	0.6
H_3PO_4	HP	7.2	44.6	36.0	2.9	0.40
	MP	7.1	65.3	–	4.8	0.68
	LP	10.2	43.8	40.6	2.0	0.20
NaOH/NaCl	HP	3.4	23.3	70.8	0.8	0.24
	MP	4.0	26.6	64.9	0.4	0.10
	LP	4.8	29.7	62.0	0.9	0.19

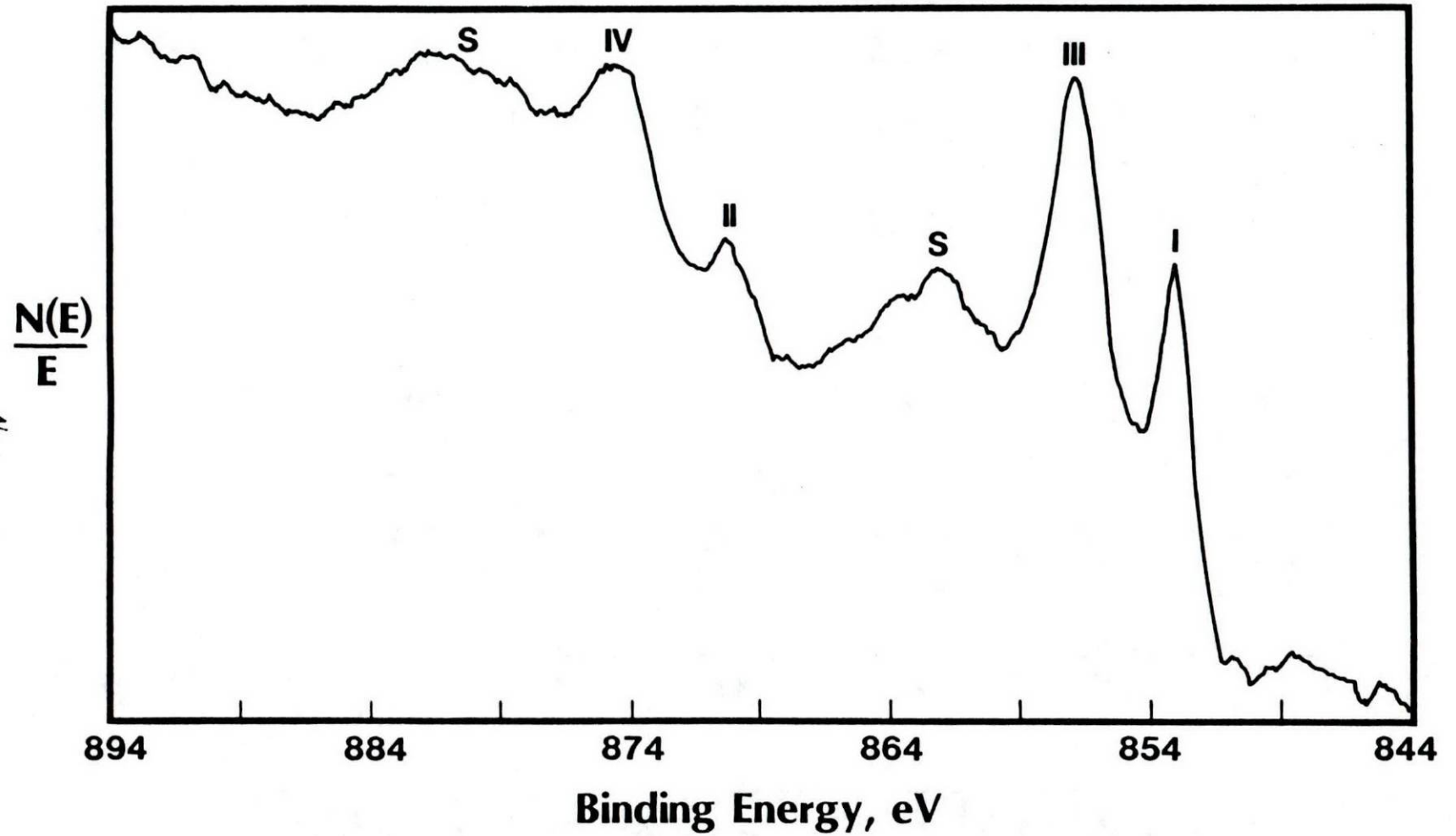

Figure 1. Representative Ni2p ESCA spectrum for the as-plated EN surface. The spectrum shown was obtained for a MP coating at a take off angle of 45°. The peak notations are explained in the text.

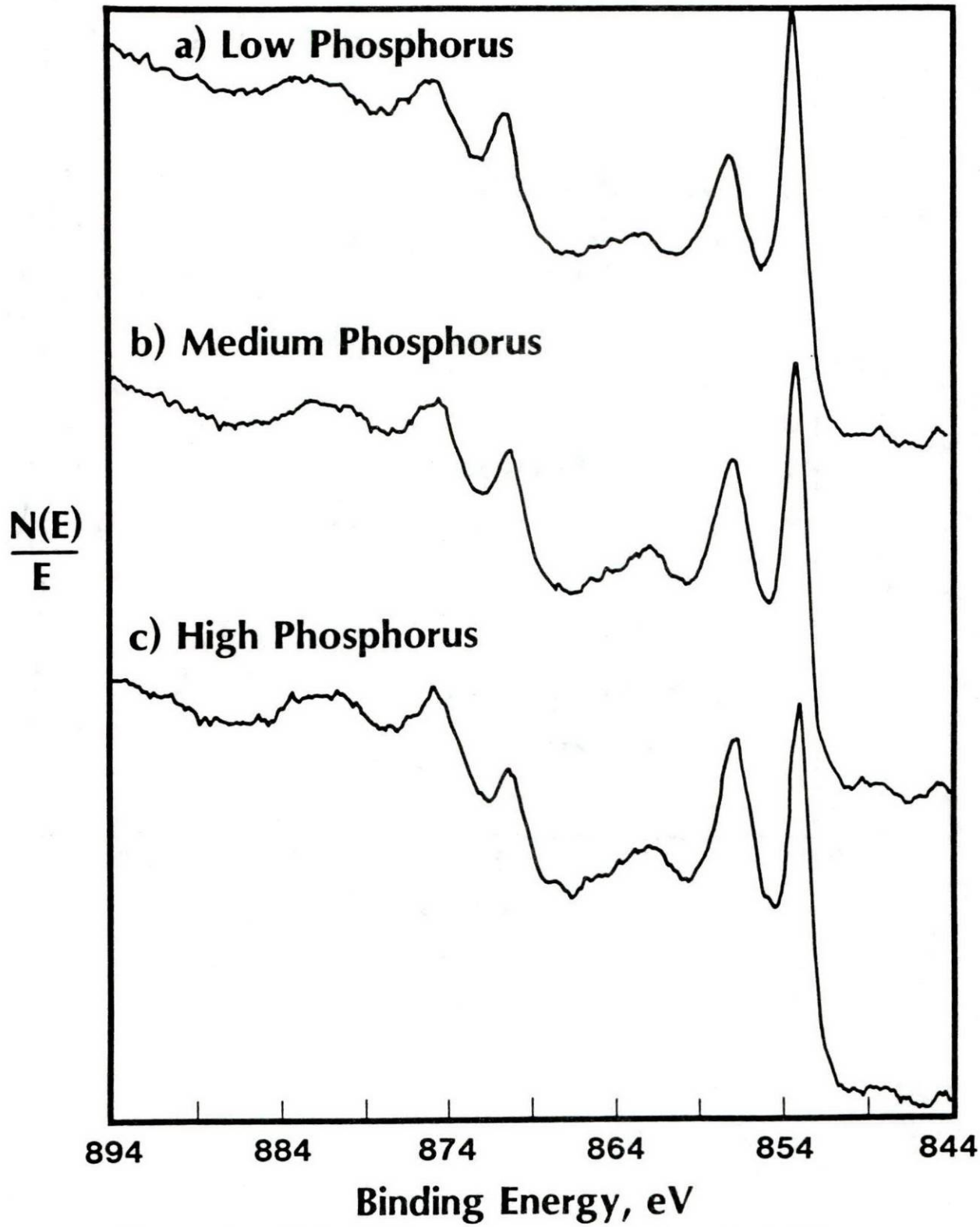

Figure 2. Ni2p ESCA spectra of as-plated a) LP b) MP and c) HP EN coatings at a 90° take off angle.

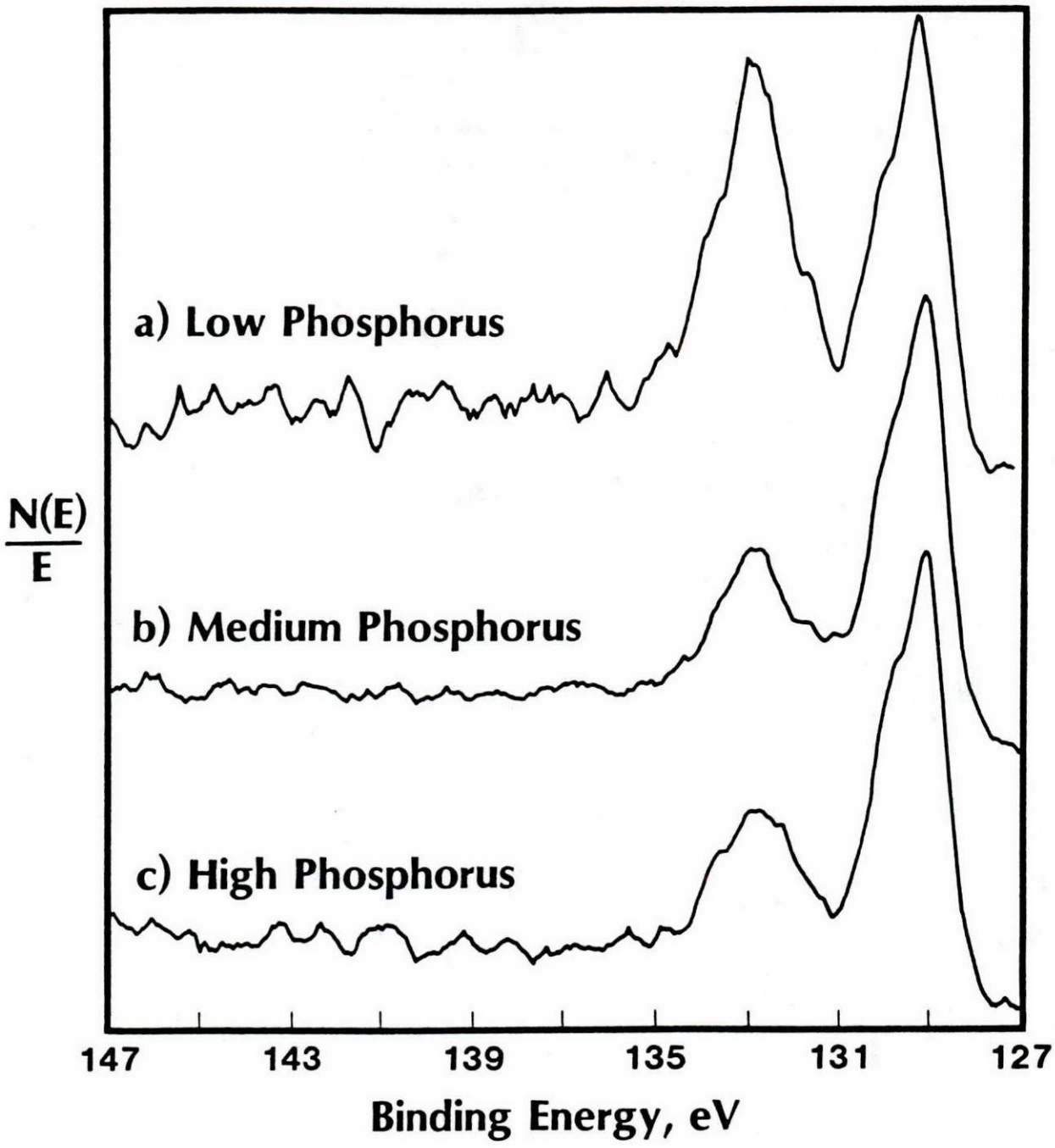

Figure 3. P2p ESCA spectra of as-plated a) LP b) MP and c) HP EN coatings at a 90° take off angle.

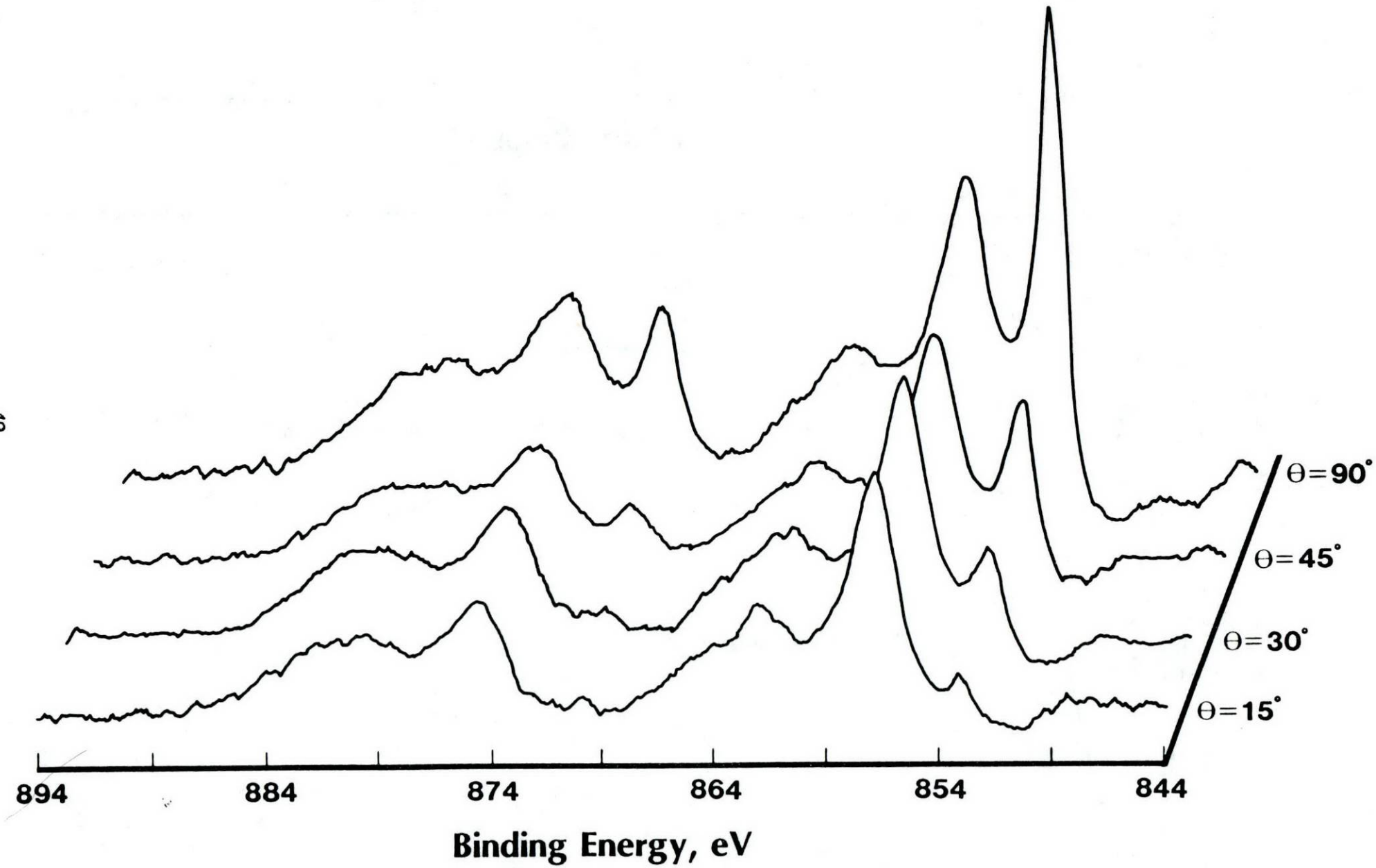

Figure 4. ADESCA Ni2p spectra collected for the as-plated MP EN coating. Spectra are shown at angles of 15°, 30°, 45° and 90°.

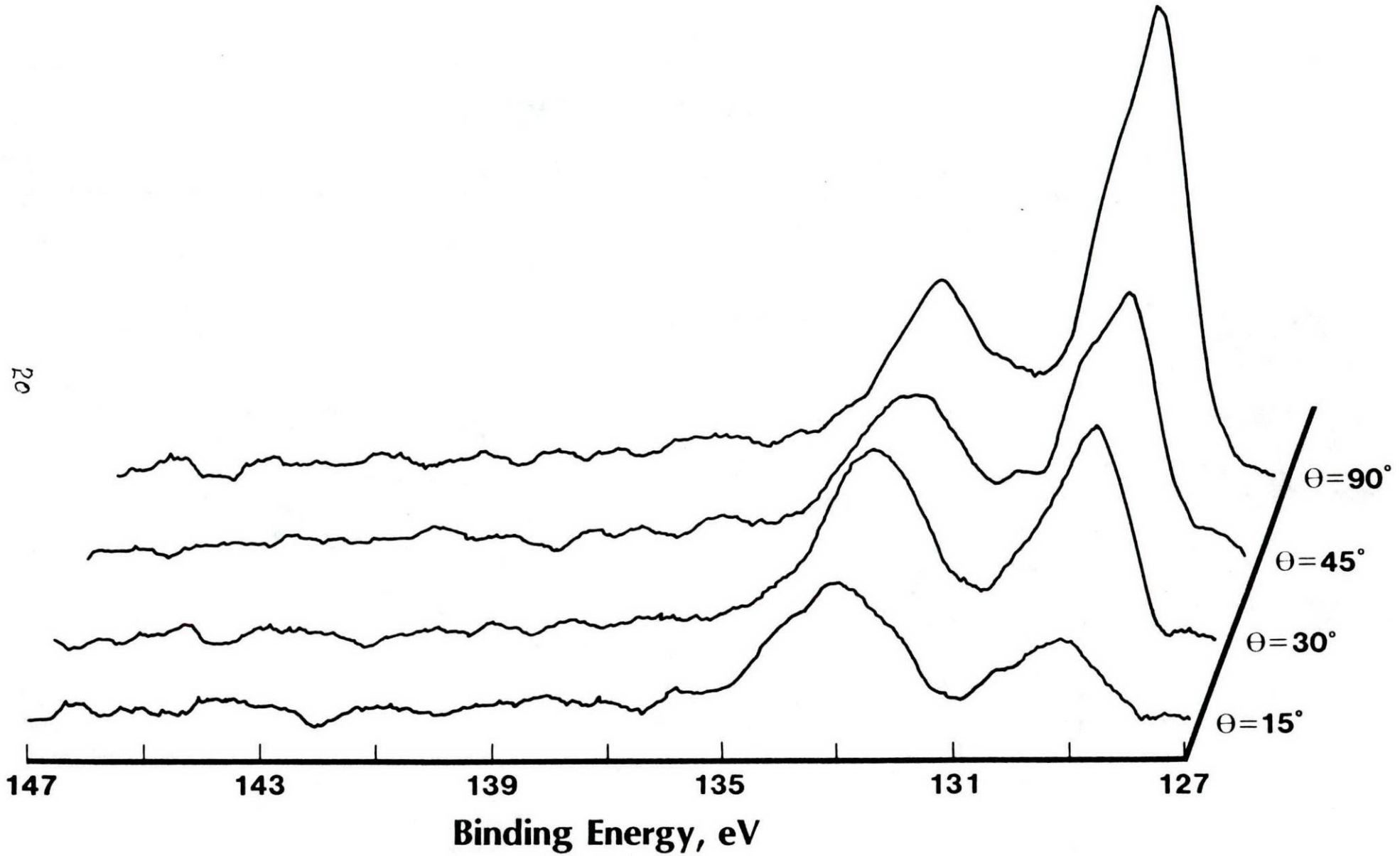

Figure 5. ADESCA P2p spectra for the as-plated MP material. Spectra are shown for take off angles of 15°, 30°, 45° and 90°.

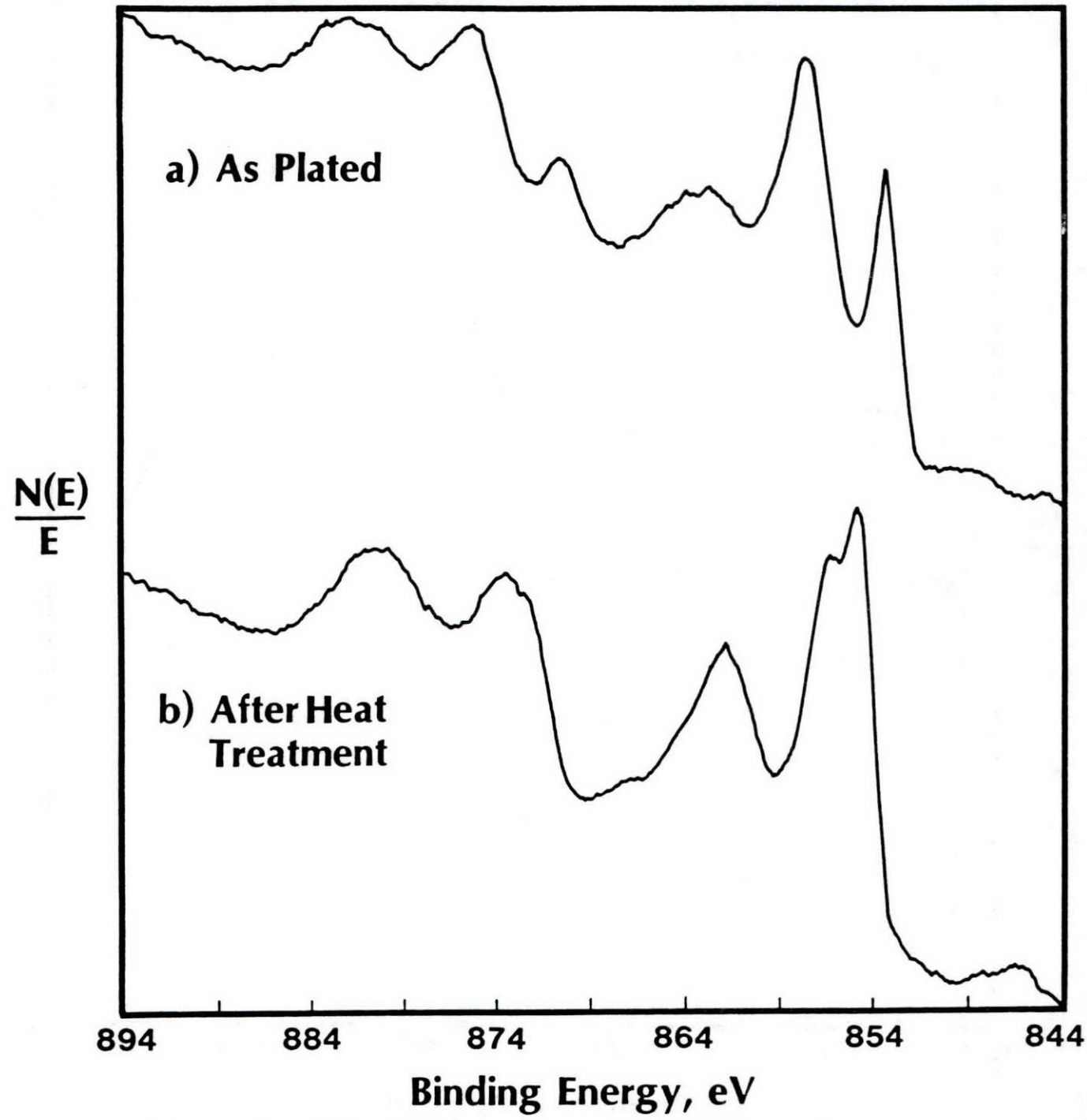

Figure 6. Ni2p ESCA spectra of a HP EN coating a) as-plated and b) after heat treatment.

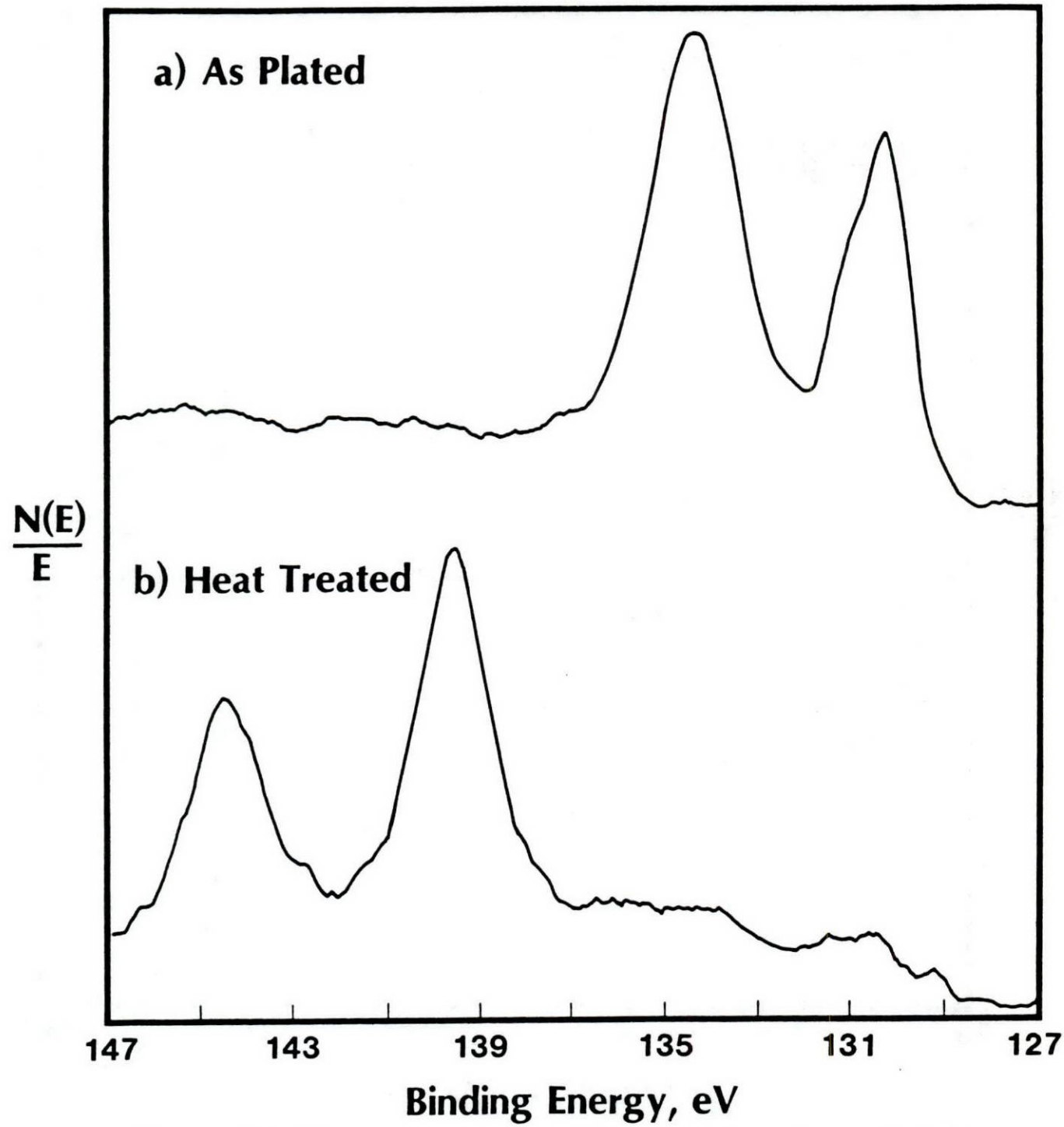

Figure 7. P2p spectra for a HP EN coating a) as-plated and b) after heat treatment.

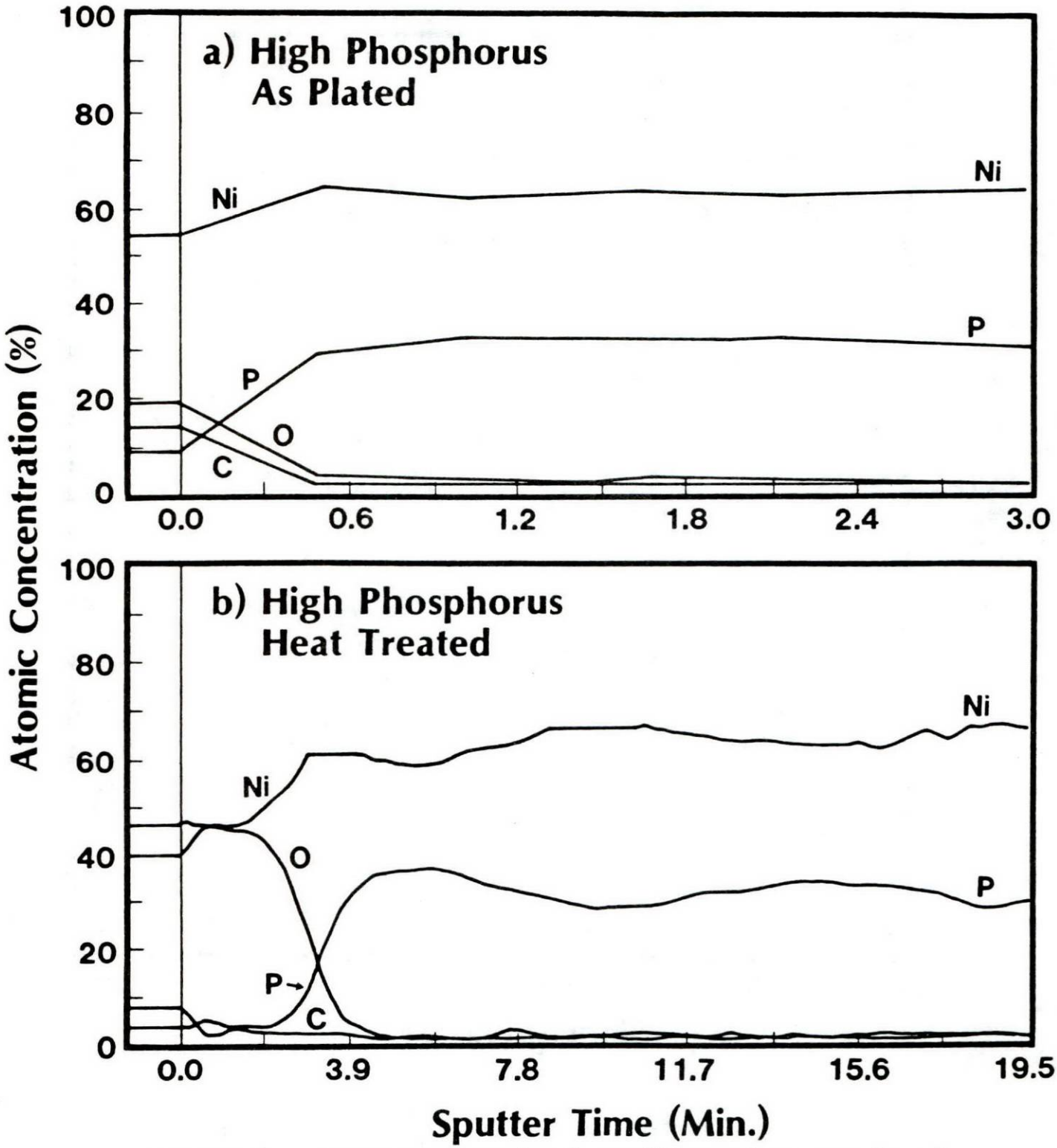

Figure 8. Auger sputter depth profiles of a) as-plated and b) heat treated HP EN. The sputter rate was 65A/min. measured relative to a SiO_2 standard.

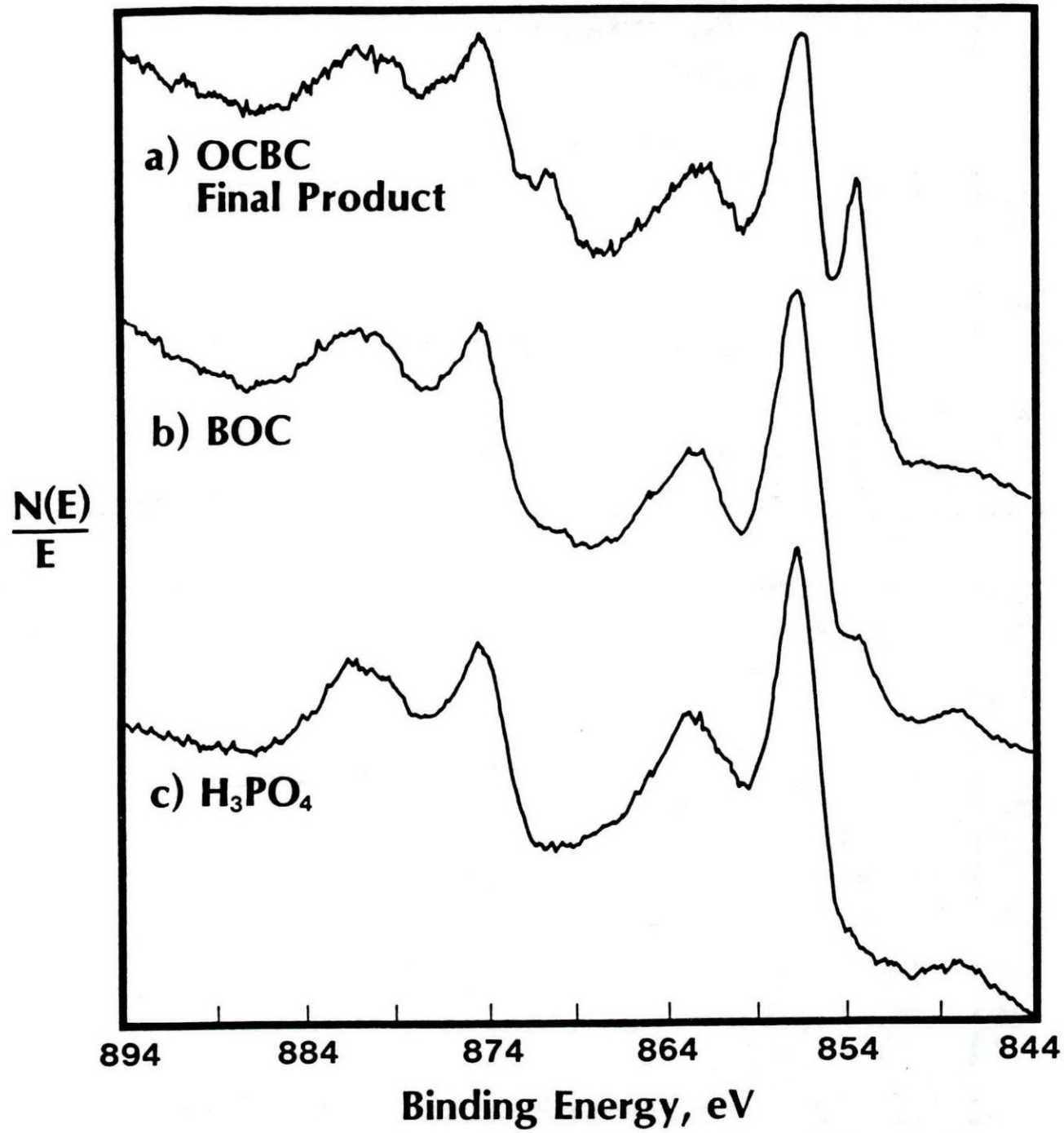

Figure 9. Examples of Ni2p ESCA spectra obtained for corrosion tested HP coatings. Spectrum a) was tested in OCBC, spectrum b) BOC and spectrum c) H_3PO_4. All of the data was collected at a take off angle of 45°.

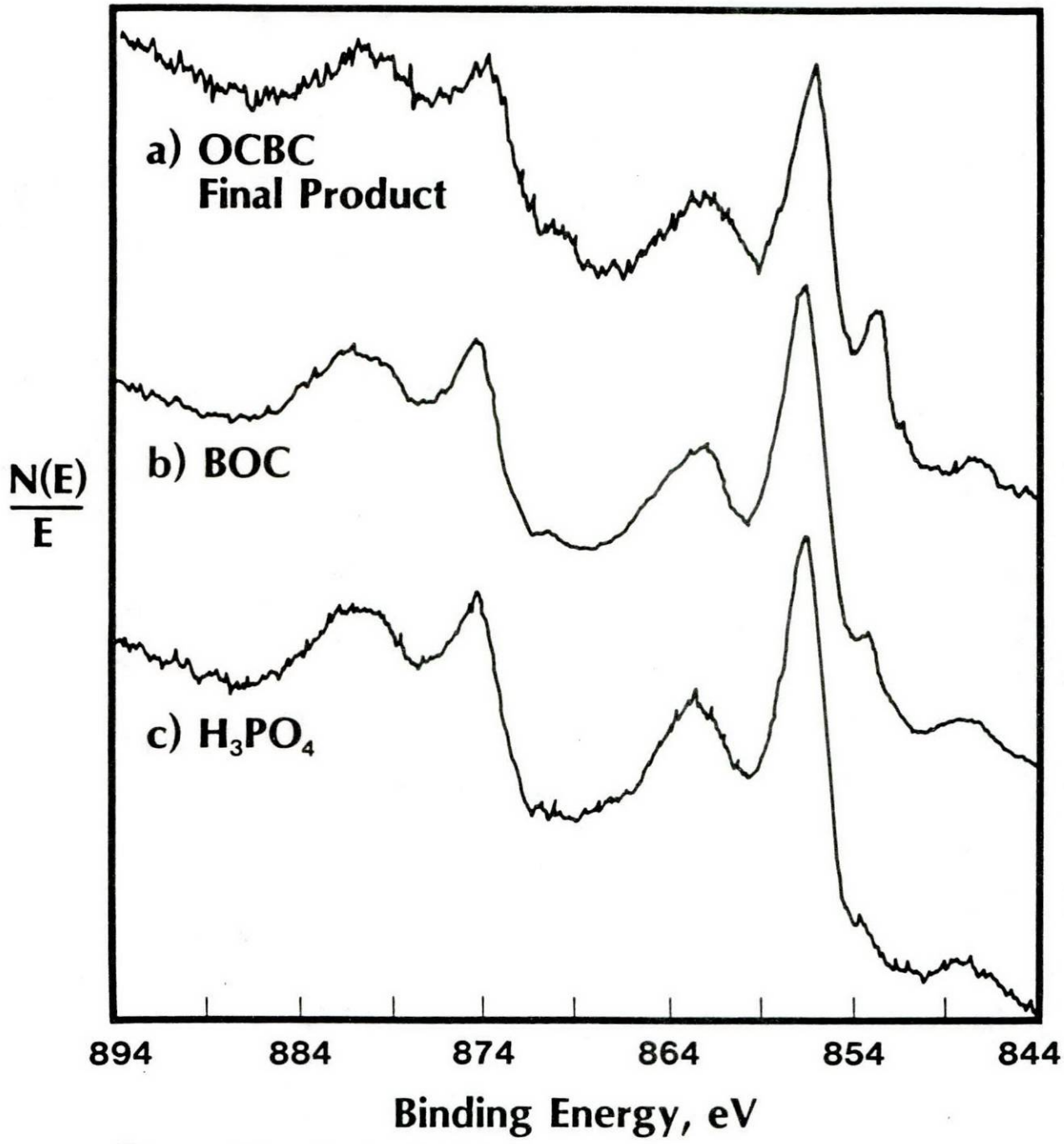

Figure 10. Typical Ni2p ESCA spectra obtained for corrosion tested LP coatings. The spectra represent coatings tested in a) OCBC b) BOC and c) H_3PO_4. All of the spectra shown were obtained at a 45° take off angle.

I-4

Electroless Deposition I
Session I

Electric Properties of Electroless Copper Deposits

Kuniaki Ohtsuka
Okuno Chemical Industries Co., Ltd.
10-25 1-chome Hanatenhigashi, Tsurumiku
Osaka Japan

Electric Properties of Electroless Copper Deposits

Kuniaki Ohtsuka
Okuno Chemical Industries Co., Ltd.
10-25 1-chome Hanatenhigashi Tsurumiku Osaka Japan

1. Introduction

Electroless copper plating is used in circuit preparation for printed wiring boards and plating for non-conductors such as plastics. Many research reports have been presented on plating bath compositions and deposit's physical properties.

Electroless copper plating has recently been applied to the preparation of high-frequency circuits, dielectric filters, etc., and is now drawing much attention.

With the increase in the quantity of information in parallel with the recent remarkable progress in the information field, electric waves and communication apparatuses have been subjected to high-frequency implementation, along with the further compactization of radiotelegraph apparatuses. Accordingly, the high-frequency filters required for such advancements also need to be compact in size and sophisticated in performance when associated with a high dielectric constant and other factors.

Such high-frequency filters have conventionally been prepared by thermally coating silver paste over dielectric ceramics with a high dielectric constant, thereby obtaining electodes.

We found that the characteristics of dielectric filters prepared by electroless copper plating are greatly affected by the bath composition, in particular by trace additives ratio. We conducted further investigations in relation to various physical properties of the deposits.

2. Experiments[1)2)]

2-1 Preparation of test pieces

2-1-1 Barium titanate ceramics

For determining high-frequency characteristic values $\eta(\%)$ of dielectric filters, electroless copper plating to 20 μm thickness was carried out for barium titanate ceramics (Fig. 2) in accordance with the process shown in Fig. 1-(a).

2-1-2 Stainless steel plates

For measuring mechanical characteristic of deposits obtained by electroless copper plating, electroless copper plating to 30 μm thickness was carried out using stainless steel plates (50 × 100 mm) in accordance with the process shown in Fig. 1-(b).

2-2 Plating baths and bath conditions

As shown in Table 1, various additives were added to the basic bath containing EDTA as a chelating agent, and the ex-

perimental baths thus obtained were used for plating experiments at 65°C.

2-3 Determination of high frequency characteristic values η(%)

Barium titanate after being subjected to 20 μm copper plating in accordance with the plating of Fig. 1-(a) was used as a band elimination filter for the high-frequency range. Frequency characteristics were measured, as shown in Fig. 3. This was followed by calculation of the value η(%) from equation (1).

$$\eta(\%) = \frac{Qu}{Qcu} \times 100 \quad \cdots\cdots\cdots\cdots\cdots\cdots \quad (1)$$

where Qu and Qcu are values representing filter fineness, Qcu being a theoretical value approximately expressed by equation (2) and Qu being calculated value by equation (3).

$$Qcu = 42 \sqrt{f_0} \times 1.8 \quad \cdots\cdots\cdots\cdots\cdots\cdots \quad (2)$$

$$Qu = 10^{\frac{L_0}{20}} \left(\frac{f_0}{f_2 - f_1}\right) \quad \cdots\cdots\cdots\cdots\cdots \quad (3)$$

where f_0 represents center frequency; $(f_2 - f_1)$ represents bandwidth at 3 dB; L_0 represents maximum attenuation quantity.

2-4 Determination of mechanical properties of deposits[3)]

Deposit film (30 μm) obtained by electroless copper plating in accordance with the plating process of Fig. 1-(b) was stripped and cut into pieces 1 cm in width and 5 cm in length. The breaking elongation and breaking tension of the test pieces were determined by means of a tensile tester (made by Shimadzu Corporation, Autograph SD-100-C).

2-5 Observation of crystal form of deposits

Using a scanning electron microscope (made by Hitachi Ltd., S-510), observations were made of the crystal form of deposits

2-6 Determination of film thickness

A copper plate 20 × 20 mm in size was plated simultaneously with each subject materrial and the film thickness was calculated by gravimetry.

3. Results and Discussion

3-1 Effects of additives on η value

Different η values were obtained depending upon type and concentration of trace additives. (Fig. 4 (a)∿(d))

When 2,2'-dipyridyl or sodium cyanide was added, η value decreased with the increase in additive concentration; value reached the maximum when 10 to 20 mg/l of 2,2'-dipyridyl was added.

The effects of various compounds used in combination with 10 mg/l of 2,2'-dipyridyl were next examined. As shown in Fig. 4-(c), the addition of thiodiglycolic acid raised η value to a high degree with the maximum being obtained at 5 mg/l concentration. When PEG #1540 (polyethylene oxide) was added, η value showed gradual decreases in proportion to the increased concentration. In the case of potassium nickel cyandide, its addition greatly reduced η values.

3-2 Effects of additives on deposition rate

When 2,2,'-dipyridyl or sodium cyanide was added, deposition rate decreased with the increase in additive concentration. In particular, 2,2'-dipyridyl had a great effect. (Fig. 5 (a) and (b))

The effects of various compounds when used in combination with 10 mg/l of 2,2,'-dipyridyl on deposition rate were then examined. As a result, PEG #1540 was found to have no considerable effect on deposition rate. However, in the case of addition of potassium nickel cyanide or thiodiglycolic acid, deposition rate showed noticeable decreases with the increase in additive concentration. In particular, when thiodiglycolic acid was added in a ratio of 30 mg/l or more, deposition rate decreased to almost zero. (Fig. 5 (c) and (d))

Comparing Fig. 5 with Fig. 4, it was conjectured that there is no correlation between deposition rate and high-frequency characteristic.

3-3 Effects of additives on mechanical properties of deposit film

When 2,2'-dipyridyl was added alone, the breaking elongation and breaking tension of deposit film both exhibited the maximum value at 20 mg/l concentration. When used in combination with 1 g/l ethylenediamine (EDA), however, breaking elongation increased while breaking tension decreased, with the increase in 2,2'-dipyridyl concentration. (Fig. 6 (a))

Fig. 6 (b), (c) and (d) present the results obtained in cases where various compounds were used in combination with 10 mg/l of 2,2'-dipyridyl. When potassium nickel cyanide or PEG #1540 was added, breaking elongation increased while breaking tension decreased, with the increase in additive concentration. When thiodiglycolic acid was added, breaking elongation and breaking tension both decreased with the increase in additive concentration.

Comparing Fig. 6 with Fig. 4, it was conjectured that there is no correlation between the mechanical properties of deposit film and the high-frequency characteristic of the obtained filter.

3-4 Relationship between additives and crystal form of deposits

When 2,2'-dipyridyl or sodium cyanide was added, deposit grain size tended to decrease with the increase in additive concentration. (Fig. 7 (a)∿(d))

EDA and thiodiglycolic acid both tended to reduce deposit grain size. In particular, EDA was noticeable in relation to such effect. (Fig. 7 (e) and (f))

Potassium nickel cyanide and PEG #1540 both tended to upgrade deposit grain size, and PEG #1540 also made deposit crystal form sharply angled. (Fig. 7 (g) and (h))

Comparing Fig. 7 with Fig. 4, it was conjectured that there is no correlation between the crystal form of deposits and the high-frequency characteristic of the obtained filter.

4. Conclusion

(1) In preparing barium titanate ceramic band elimination filters for high-frequency waves by electroless copper plating, filter characteristics are greatly affected by the trace additives in plating bath; it has become possible to obtain highly reliable dielectric filters by selecting a suitable bath composition.

(2) It was found that there is no correlation between the high-frequency characteristic of ceramic filters prepared by electroless copper plating and the mechanical properties or crystal form of the deposit film.

Reference

1. L. G. Bhatgadde and S. Mahapatra, Metal Finishing, 85, 55

2. Donald W. Bardrand, Metal Finishing, 85, 115

3. S. Yamato and M. Tadakoshi, Metal Finishing, 85, 67

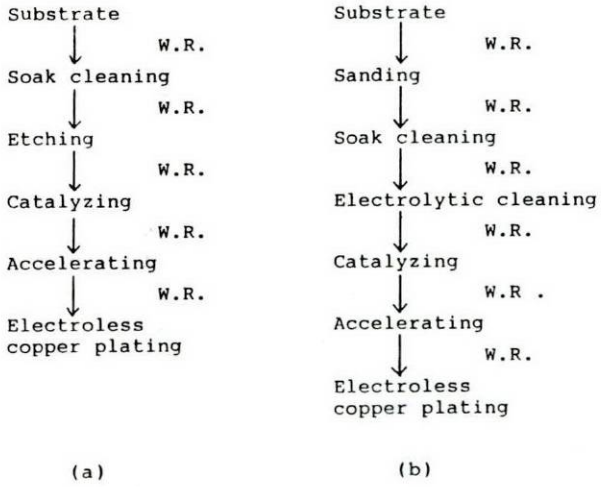

Fig. 1 Plating processes

(a) is the plating process for barium titanate ceramics and (b) is the plating process for the stainless steel.

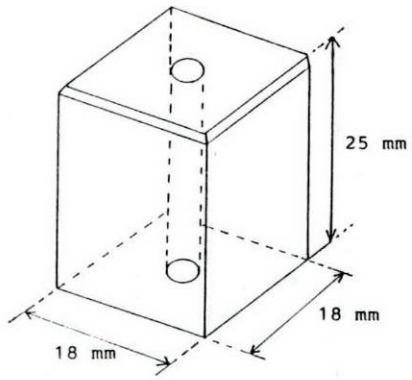

Fig. 2 Test piece

Barium titanate ceramics for measurements of the high frequency characteristic

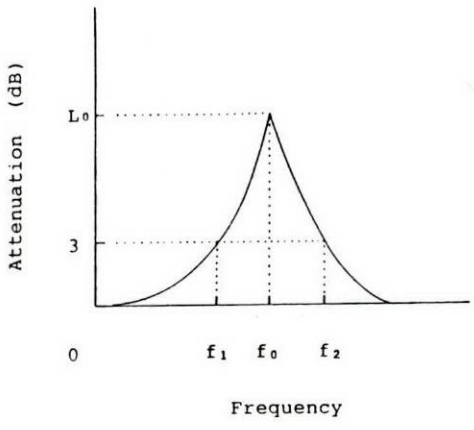

Fig. 3 A rough sketch of frequency characteristic curve.

The base of plating bath compositions	NaOH	10 g/l
	$CuSO_4 \cdot 5H_2O$	10 g/l
	EDTA · 2Na · $2H_2O$	30 g/l
	HCHO	4 g/l
Aditives	NaCN	0 - 100 mg/l
	$K_2Ni(CN)_4$	0 - 100 mg/l
	2,2'-dipyridyl	0 - 100 mg/l
	Tiodiglycolic acid	0 - 100 mg/l
	PEG #1540	0 - 3 g/l
	Ethylenediamine	0 - 1 g/l

Table 1. Plating bath compositions

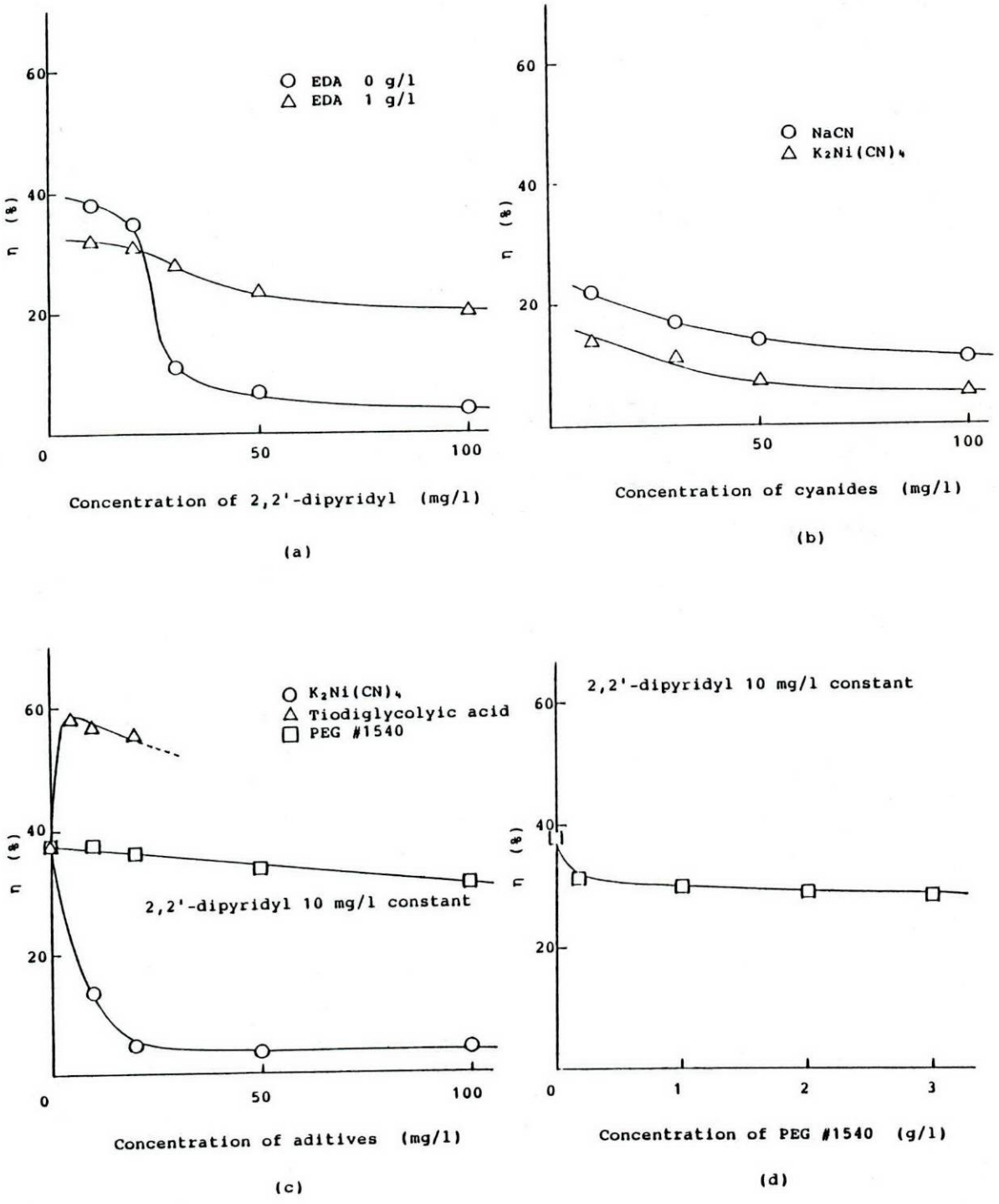

Fig. 4 The relation between the aditives and the high frequency characteristic.

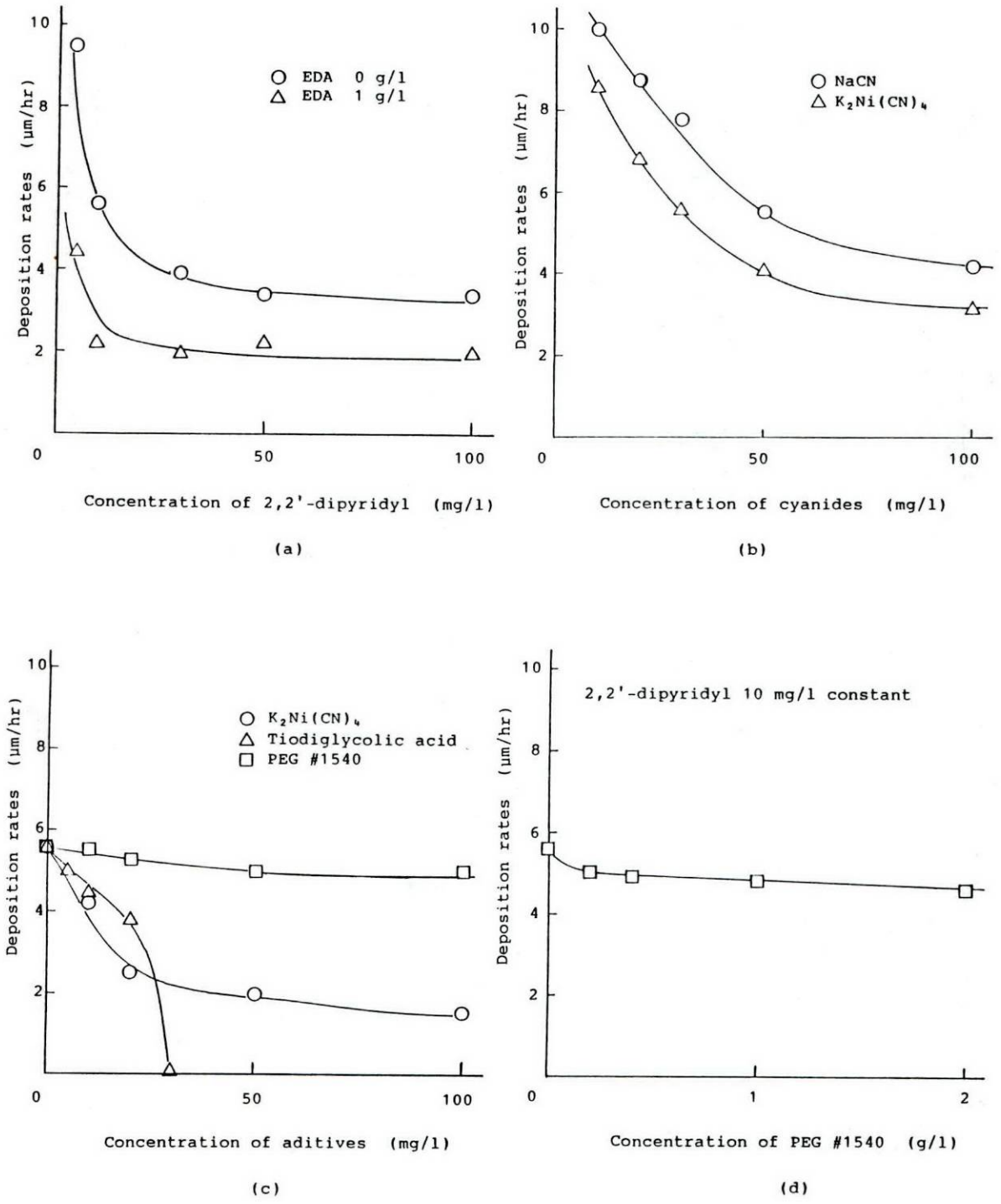

Fig. 5 The relation between the aditives and the deposition rates.

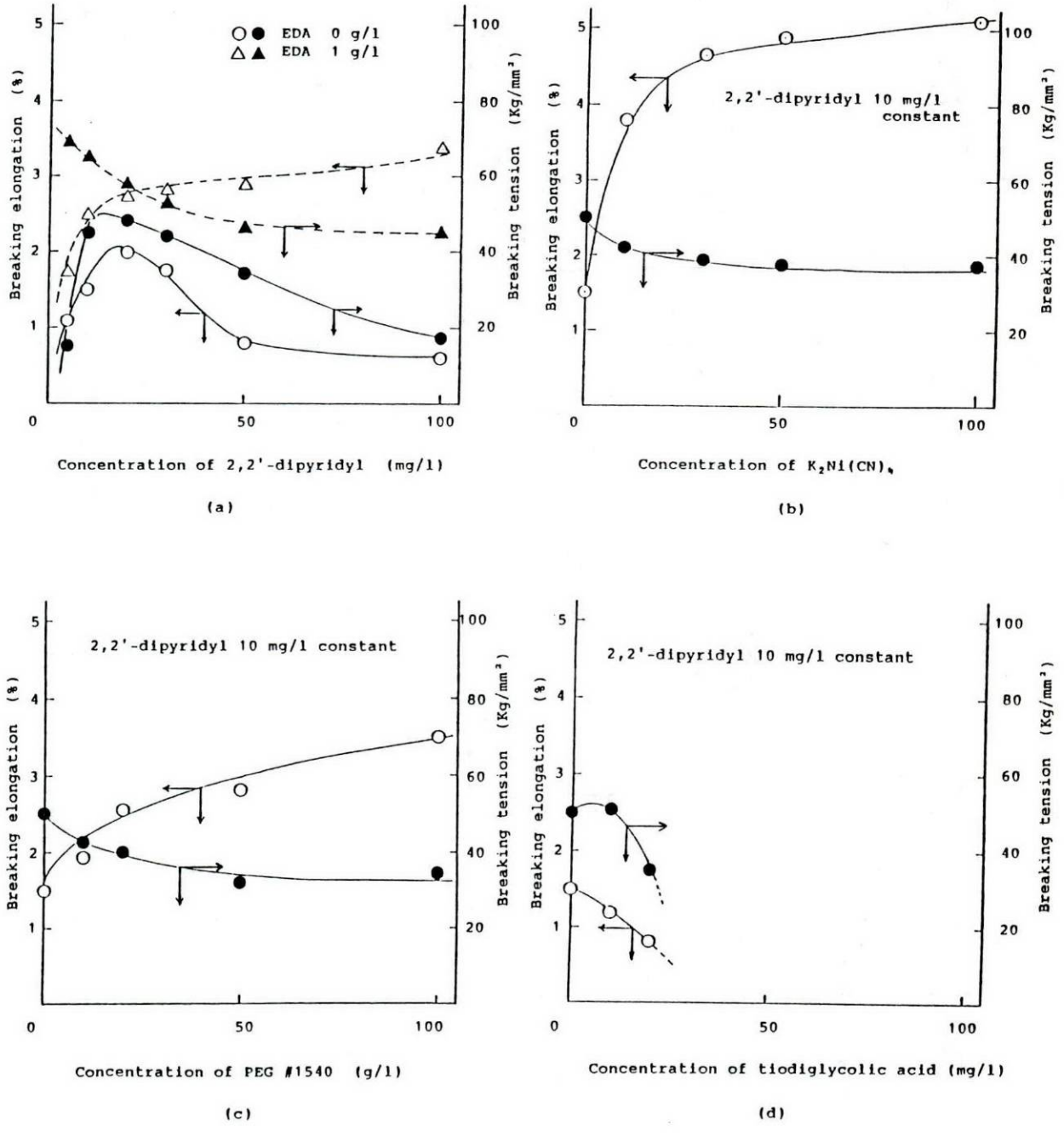

Fig. 6 The relation between the aditives and the mechanical property of deposits.

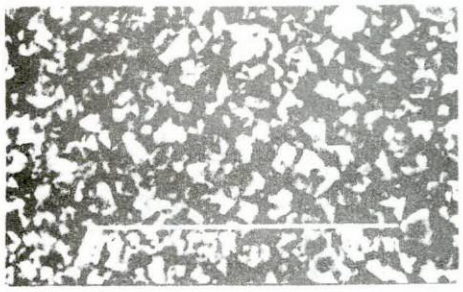

(a) 2,2'-dipyridyl 10 mg/l

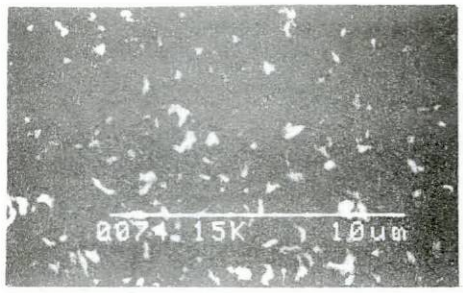

(b) 2,2'-dipyridyl 100 mg/l

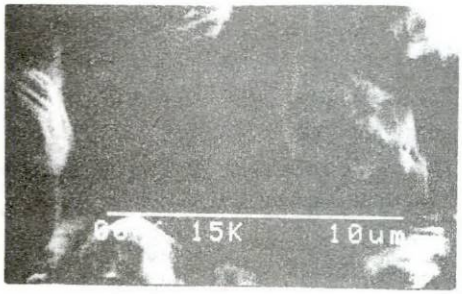

(c) NaCN 10 mg/l

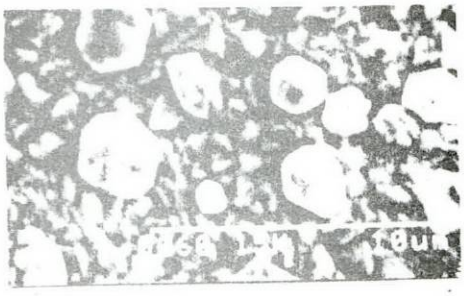

(d) NaCN 100 mg/l

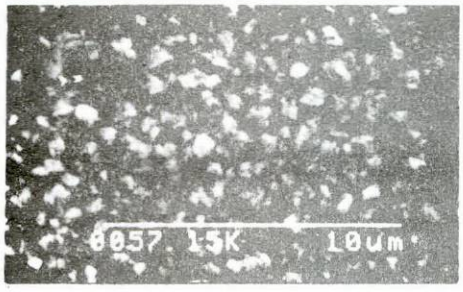

(e) 2,2'-dipyridyl 10 mg/l
Tiodiglycolic acid 5 mg/l

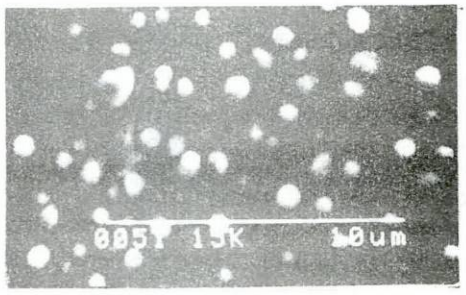

(f) 2,2'-dipyridyl 10 mg/l
EDA 1 g/l

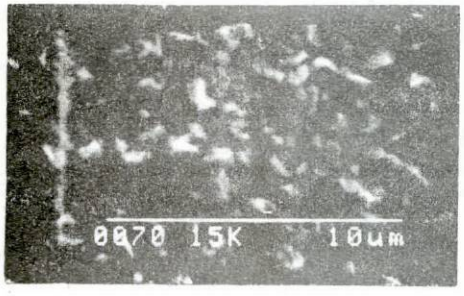

(g) 2,2'-dipyridyl 10 mg/l
$K_2Ni(CN)_4$ 10 mg/l

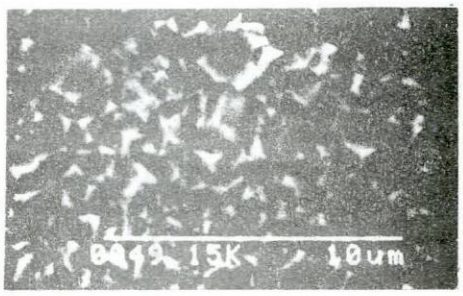

(h) 2,2'-dipyridyl 10 mg/l
PEG #1540 1 g/l

Fig. 7 The crystal form of deposits

I-5

Electroless Deposition I
Session I

Some Physical Properties of Electroless Ni-P Alloy Deposited from Pyrophosphate Bath

Masao Matsuoka, Shinji Imanishi
and Tadao Hayashi
Department of Applied Chemistry
University of Osaka Prefecture
4-804 Mozu-Umemachi, Sakai
Osaka, 591, Japan

Some Physical Properties of Electroless Ni-P Alloy Deposited from Pyrophosphate Bath

Masao Matsuoka, Shinji Imanishi, Tadao Hayashi

Department of Applied Chemistry, University of Osaka Prefecture
4-804 Mozu-Umemachi, Sakai, Osaka, 591, Japan

Abstract

Some physical properties of the Ni-P alloys prepared from an ammoniacal pyrophosphate bath were examined as a function of P content. The higher P content gave rise to the lower internal stress of Ni-P alloys. The resistivity of Ni-P deposits was found to decrease with decreasing the P content and also by the heat-treatment. The precipitation of Ni_3P induced by the heating remarkably increased the hardness of Ni-P alloys. Changes in physical properties attributable to the alteration of P content and heating were discussed in view of the crystallographic feature of Ni-P alloys.

1. Introduction

It is well known that Ni-P alloys with higher phosphorus content are deposited from acid electroless nickel bath by using hypophosphite as a reducing agent. In particular, the Ni-P alloys of which phosphorus content is greater than 10 wt.% show the characteristic properties due to the amorphous structure, i.e., the high performance of corrosion resistance and hardness. As the amorphous Ni-P alloys have non-magnetic properties, they could be applied to the undercoating of aluminum substrates for the fabrication of magnetic memory disks, in addition to the usage of corrosion and wear resistant coatings[1]. However, the higher deposition rate suitable for the practical use could not be obtained unless operating temperature was greater than 90°C. Therefore, the use of acid electroless nickel plating bath seemed to be somewhat restricted. On the other hand, an ammoniacal electroless nickel bath was generally operated at fairly low temperature and used for the metallization of plastic substrates. The physicochemical properties of the Ni-P alloys deposited from an alkaline bath do not seem to be fully elucidated. Therefore, an ammoniacal pyrophosphate bath that could be operated at 50 to 70°C was employed for the further study and the physical properties of the Ni-P deposits, such as internal stress, hardness and resistivity were examined as a function of phosphorus content of the deposits.

2. Experimental

2.1 Deposition Rate of Ni-P Alloys and Phosphorus Content

The bath composition and operating conditions for the electroless nickel plating are shown in Table 1. Platinum strips (10 cm^2) used as the substrates were electrodegreased and activated by the solution of $PdCl_2$. The platinum substrates were immersed in the electroless nickel bath with a volume of

250 ml for 30 min, and then the deposition rate of Ni-P alloys was estimated by the weight gain during the plating. The phosphorus content was determined by dissolving a known amount of Ni-P alloys in a solution of 1 M HNO_3. Phosphorus was completely oxidized to orthophosphate by the use of potassium permanganate. An adequate amount of ammonium vanadate and ammonium molybdate were added as color indicator and then absorbance of the solution was measured at 460 nm[2].

2.2 Heat-treatment and X-ray Diffraction

Heating of the sample was carried out in vacuum (5×10^{-4}) at 400 °C for 1 h. The hardness and crystallographic structure of Ni-P alloys were examined before and after the heat-treatment. CuKα radiation (45kV, 50mA) was used for the X-ray diffraction analysis. The Ni-P alloys deposited on copper substrates with a thickness of 20 μm were tested. Apparent crystallite size of the deposits was estimated by Scherrer's equation ($0.89\ \lambda\ /\ \beta_{\frac{1}{2}}\ \cos\ \theta$)[3]. In the case of heat-treated sample, the amount of nickel phosphide was qualitatively evaluated by the intensity of the diffraction line due to Ni_3P.

2.3 Physical Properties of Ni-P Alloys

Copper strips (9 x 1 cm) from which strain was eliminated by annealing in vacuum were employed for the measurement of internal stress of Ni-P alloys. One side of the copper strips was covered with thin scotch tape, and then electroless Ni-P alloys were plated on the other side of the substrate until thickness reached to 10 μm. The bowing caused by the internal stress of the deposits was measured by using a micrometer. The values of the stress were calculated by the following equation[4].

$$S = 4\ E\ d^2 Z/(3\ t\ L^2) \quad \text{--- (1)}$$

where, E is Young's modulus of copper substrates, d thickness of substrates, Z bowing created by the stress, t thickness of Ni-P alloys, and L length of substrates.

The hardness of the Ni-P alloys was measured for the sample with a thickness of 20 μm by using a Shimazu micro vickers hardness tester with a load of 50 g.

The resistivity of Ni-P alloys was determined with a portable double-bride device at room temperature. The Ni-P alloys with a thickness of 2 μm were plated on a cylindrical ceramic substrate which was received by the following conventional pre-treatment: degreasing in an alkaline solution - etching (dichromic acid/sulfuric acid) - sensitizing ($SnCl_2$) - activation ($PdCl_2$).

3. Results and Discussion

3.1 Plating Rate and P Content as a Function of pH or Temperature

As can be seen in Fig.1, the deposition rate of nickel strongly increased when bath pH was increased from 10 to 12, but the deposition rate of phosphorus was independent of bath pH. The phosphorus content, therefore, decreased from 7.3 wt.% to 3.0 wt.%. These results indicate that the reduction of nickel is

much more favorable than the co-deposition of phosphorus under the conditions of high pH. The same tendency has already been reported for the acid electroless nickel plating[5].

The deposition rate of nickel and phosphorus increased exponentially with an increase in operating temperature as shown in Fig.2. The apparent activation energy calculated from the temperature dependence of the deposition rate of nickel and phosphorus was found to be 7 kcal/mole in each case. The phosphorus content of Ni-P alloys was, therefore, independent of bath temperature within the range between 50 °C and 70 °C. The apparent activation energy evaluated from the Schartz's data reported for an ammoniacal pyrophosphate bath was 10 kcal/mole[6]. In general, the value of the activation energy for the deposition of Ni-P alloys was fairly smaller in ammoniacal electroless nickel bath than that in acid bath (17.7 kcal/mole). This fact seemed to be one of the reason that the higher deposition rate could be expected in the case of ammoniacal electroless nickel bath[7]. As described above, if the activation energy for the deposition of nickel and phosphorus was identical, the phosphorus content is independent on temperature. However, it has been found that the temperature dependence of phosphorus content was quite different with bath pH employed[8]. It should be noticed that the activation energy for the deposition of nickel and phosphorus was influenced by the plating conditions. The effect of some additives on the deposition rate of phosphorus has been examined by Feldstein[9]. Through the study, a new mechanism for the deposition of phosphorus via PO_2^- has been proposed instead of one electron reduction from hypophosphite, because the slope of the line obtained by plotting the logarithmic value of the deposition rate of phosphorus against the mixed potential indicated the reduction via 3 electrons. However, this postulation is not yet generally accepted.

3.2 Crystallographic Structure of Ni-P Alloys

Typical X-ray diffraction lines of the Ni-P alloys with a composition of 7.3 wt.% P is shown in Fig.3. As-plated Ni-P alloys gave a diffused line at the angle corresponding to Ni(111). It has been confirmed that the broadness increases by an increase in phosphorus content. The apparent crystallite size evaluated from the half-width of the diffraction line by using Scherrer's equation decreased from 119 Å to 14 Å, when phosphorus content increased from 3.0 to 7.3 wt.%. On the other hand, the heating of the Ni-P alloys resulted in produced the re-crystallization of nickel as well as the formation of Ni_3P. It has been confirmed that the intensity of diffraction lines corresponding to Ni_3P increase with increasing the phosphorus content. The crystallographic structure of Ni-P alloys was remarkably influenced by the phosphorus content of the deposits. The broadness of the diffraction line as recognized in the case of as-plated Ni-P alloys was due partly to micro-crystalline structure and partly to the amorphous structure of the deposits. On this point, it has been disclosed by Cargill[10] that Ni-P

alloys became complete amorphous structure in the case of the electrodeposited Ni-P alloys. The contribution of amorphous structure seemed to become dominant when the phosphorus content of the electroless Ni-P alloy increased. The amorphous structure was not stable at 400 °C. Therefore, the heating of the Ni-P alloy deposits yielded the re-crystallization of nickel with the formation of nickel phosphide. Changes in crystallographic structure owing to the heating and also changes in phosphorus content of the Ni-P alloy deposits remarkably influenced the properties of the deposits as will be discussed in the following section.

3.3 Internal Stress of Ni-P Alloys

In general, the internal stress of the Ni-P alloys was characterized by the tensile or compressive nature. All the internal stress observed in this study was found to be tensile stress. The high tensile stress of electroless Ni-P alloys deposited from a pyrophosphate bath was pointed out by Parker[8]. In addition, it has been found by Bartlett [11] that the internal stress of Ni-P alloys was reduced by saccharin and ferrous ammonium sulfate in the plating bath[4]. However, the relationship between internal stress and phosphorus content was not yet established. Changes in internal stress of Ni-P alloys was examined as a function of phosphorus content of the deposits. The values of internal stress of Ni-P alloys deposited from the pyrophosphate bath with different pH and temperature are shown in Fig.4. The internal stress of the Ni-P alloy (7.3 wt.%P) deposited from a bath with pH 10 was found to be 13.5 kg/mm^2 . The internal stress of the Ni-P alloy deposited from a bath with pH 11 increased to 44.7 kg/mm^2, however, the phosphorus content of the deposits decreased to 3.3 wt.% under these conditions. Further increase in bath pH did not yield any appreciable change in the internal stress of the deposits. On the other hand, the internal stress of Ni-P alloys was independent on bath temperature between 50 °C and 70 °C. Changes in phosphorus content of Ni-P alloys was found to be insignificant, therefore, the internal stress of Ni-P alloys took an almost constant value (44.3-47.1 kg/mm^2). The phosphorus content and internal stress of Ni-P alloys were remarkably influenced by bath pH, but they were not affected by operating temperature. The values of internal stress of Ni-P alloys are shown in Fig.5 as a function of phosphorus content. It is evident that the internal stress of Ni-P alloys decreased with an increase in phosphorus content of the deposits. The correlation coefficient of the data shown in Fig.5 was found to be 0.89. This result was comparable to the Parker's results obtained from acid electroless nickel bath[11]. Such a change in internal stress of Ni-P alloys was mainly due to the changes in crystarographic structure caused by alteration of phosphorus content. According to Weil[12], one of the origins for causing internal stress was impurity incorporated into the grain boundaries of the deposits. However, a number of grain boundaries attributable to the stress inducing source might be

reduced by the amorphous structure of the deposits with an increase of phosphorus content. Sugita[13] pointed out that nickel phosphite was co-deposited into Ni-P alloys as an impurity under the conditions of low pH and high hypophosphite concentration. Under these conditions, the crystallinity of the deposits decreased. Since the effect of impurity might be neglected under the conditions tested in this study, the excellent correlation between internal stress and phosphorus content was established.

3.4 Hardness and Resistivity of Ni-P Alloys

The hardness of Ni-P alloys before and after the heat-treatment is shown in Fig.6 as a function of phosphorus content. The hardness of as-plated Ni-P alloys was fairly greater than that of electrodeposited nickel. The hardness was found to be 650-685 Hv, and its value slightly increased by an increase in phosphorus content. The hardness of Ni-P alloys increased to 1000-1170 Hv by the heating at 400°C, since the phosphorus existing as supersaturated solid solution in nickel matrix crystallized to Ni_3P. The main reason for improvement of the hardness was confirmed to be deposition hardening due to Ni_3P precipitation. It has been confirmed that the harder deposits could be obtained, the higher the phosphorus content of Ni-P alloys.

The high performance of Ni-P alloys as a resistor was also well known[14]. The changes in resistivity of Ni-P alloy before and after the heating are shown in Fig.7. The resistivity of as-plated Ni-P alloys increased from 60 to 110 μΩ cm by increasing the phosphorus content. The free mean path of conducting electron decreased by increasing phosphorus content of Ni-P alloys. Therefore, the resistivity was much greater than that of pure nickel (7.24 μΩ cm). In the case of amorphous alloy, the value of resistivity was found to be 50-350 μΩcm, which is greater than that of crystalline state by a factor of 10 to 100. In addition, the temperature coefficient of resistivity (TCR) took a very small value[15]. However, the values of the resistivity of Ni-P alloys decreased by a factor of 2 to 3 by the heating, since re-crystallization of nickel and formation of Ni_3P might occur under these conditions.

3.5 Crystallite Size and Physical Properties of the Ni-P Alloys

The physical properties of the Ni-P alloys were influenced by the alteration of crystarographic feature induced by heating and also by changes in phosphorus content of the deposits. The apparent crystallite size calculated from equation (1) was taken as a measure of structural change. The resistivity and also internal stress of Ni-P alloys were plotted against apparent crystallite size, as shown in Fig.8. The internal stress was almost constant (40 kg/mm^2) when crystallite size was greater than 60 Å. However, the small value of internal stress was obtained at crystallite sizes less than 60 Å. The resistivity of Ni-P alloys measured before and after the heat-treatment decreased exponentially with increasing crystallite size of the Ni-P alloys. These results can be explained by the disorder of

nickel atom due to the codeposition of phosphorus inducing the reduction of mean free path of conducting electron.

4. Conclusions

Physical properties of Ni-P alloys prepared from ammoniacal pyrophosphate bath have been discussed as a function of bath pH and operating temperature.

1) The deposition rate of nickel increased with increasing bath pH, but the deposition rate of phosphorus was independent of pH. As the result, the phosphorus content decreased significantly with increasing bath pH.

2) The deposition rate of both nickel and phosphorus increased exponentially with increasing operating temperature. The activation energy for the deposition of both nickel and phosphorus was found to be identical. Therefore, the phosphorus content was not influenced by operating temperature.

3) The internal stress of Ni-P alloys shows tensile nature, and its value decreased with an increase in phosphorus content.

4) The hardness of as-plated Ni-P alloys was found to be 650-685 Hv. However, the heat-treatment of the deposits increased the hardness to 1000-1200 Hv due to the deposition hardening.

5) The resistivity of as-plated Ni-P alloys was found to be 60-110 μΩ cm. The smaller crystallite size of the deposits gave rise to the greater resistivity. The re-crystallization of the Ni_3P alloy deposits induced by the heating reduced the resistivity by a factor of 2 to 3.

References

1) T. Osaka, I. Koiwa, J. Metal Finishing Soc., Japan, 34, 330 (1983)
2) U. George, H.Merk, A.F.Bogenschutz, Galvanotechnik, 72, 586 (1981)
3) G.O.Mallory, Plating and Surf. Finish., 63, 34 (June 1976)
4) B.C.Bartlett. L.Cann. J.Hayward. Plating, 56, 168 (1969)
5) Ed., F.Lowenheim, "Modern Electroplating", p.710 (John Willey & Sons, Inc.)(1974)
6) M. Schartz, Proc., Am. Electroplat. Soc., 47, 176 (1960)
7) S. Ishibashi, "Mudenkai Mekki", p.69 (Asakura, 1971)
8) K. Parker, H. Shah, Plating, 58, 230 (1971)
9) N. Feldstein, T.S.Lancsek, J. Electrochem. Soc., 118, 869 (1971)
10) G.S.Cargill, J. Appl. Phys. 41, 12 (1970)
11) K. Parker, H.Shah, J. Electrochem. Soc., 117, 1091 (1970)
12) R. Weil, Plating, 58, 137 (1971)
13) K. Sugita, N. Ueno, J. Electrochem. Soc., 131, 111 (1984)
14) M. Fernandez, J. M. Martinez-Duart, J. M. Albella, Electrochim. Acta, 31, 55 (1986)
15) K. Masumoto, K. Fukamichi, " Amorufasu Goukin", p.208 (Agune,1984)

Table 1 Bath composition and operating condition

$NiCl_2 \cdot 6H_2O$	24	g/L
$Na_4P_2O_7 \cdot 10H_2O$	50	g/L
$NaH_2PO_2 \cdot H_2O$	20	g/L
pH (with NH_4OH)	11	
Temp.	60	°C

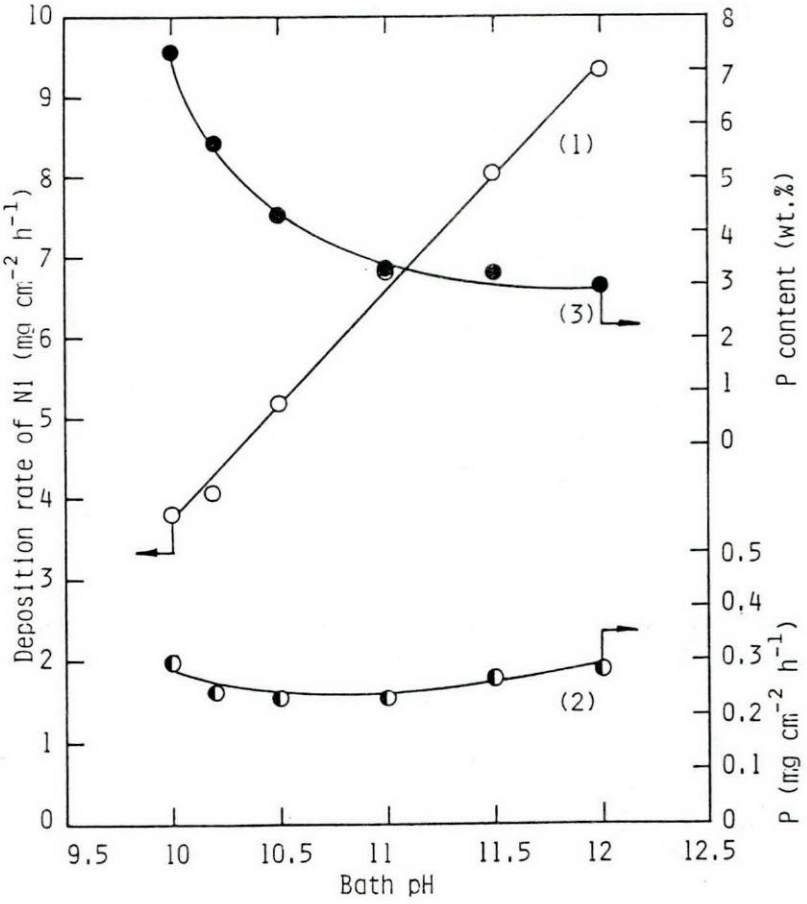

Fig.1 Effect of pH on P content and the deposition rate of Ni and P
(1) Ni, (2) P, (3) P content

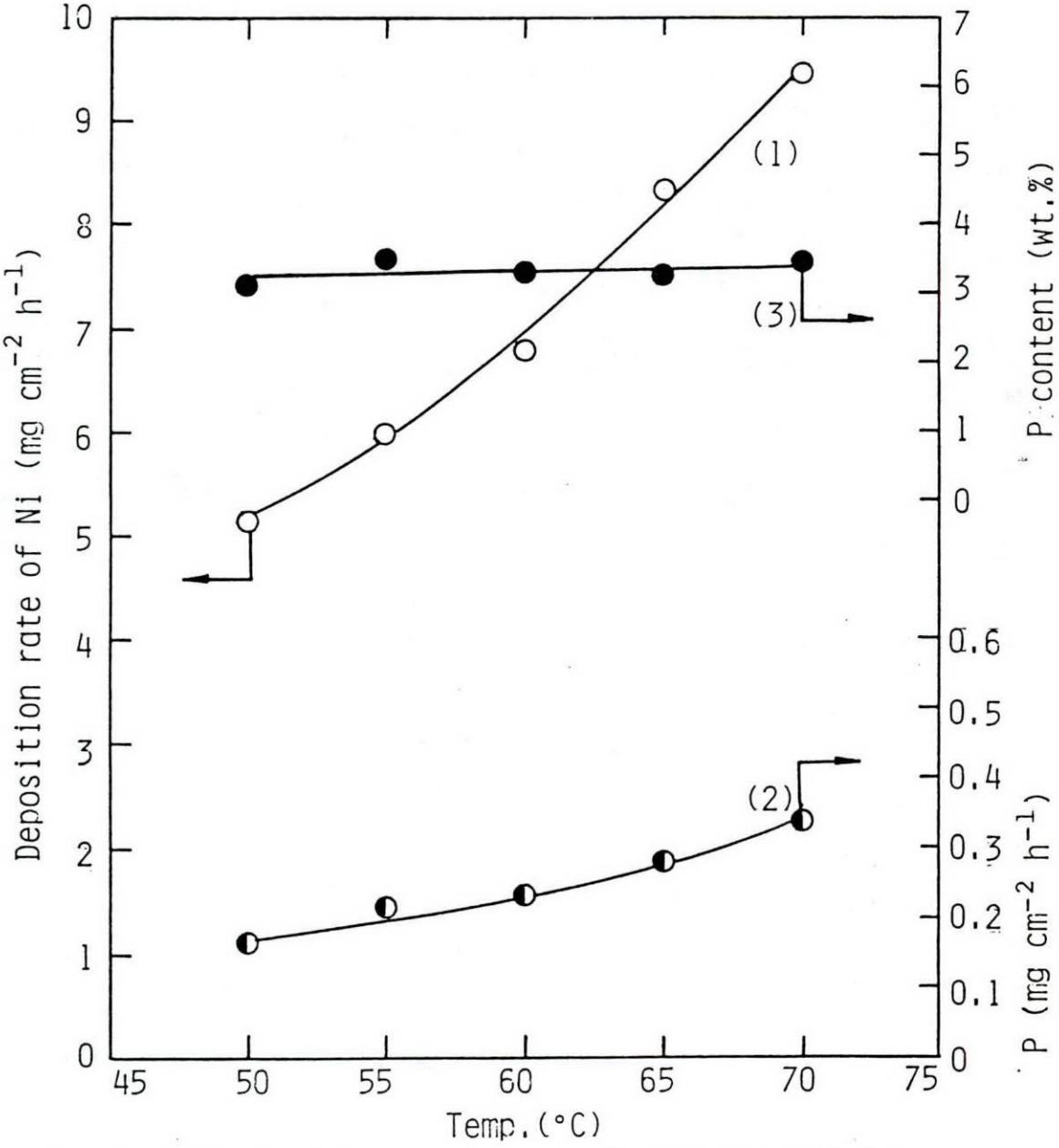

Fig.2 Effect of temperature on P content and the deposition rate of Ni and P
(1) Ni, (2) P, (3) P content

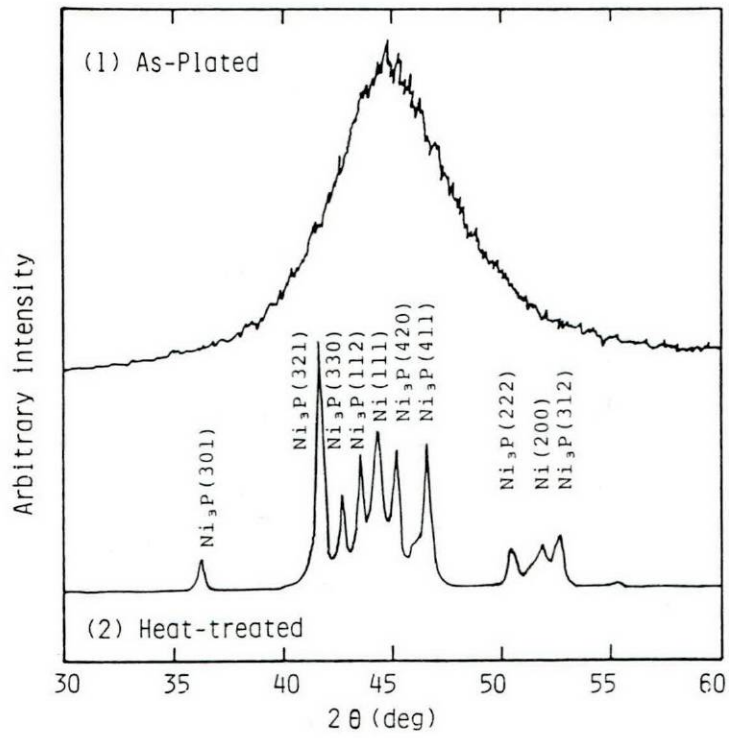

Fig.3 Typical X-ray diffraction patterns of Ni-P deposit (7.3 wt.% P)

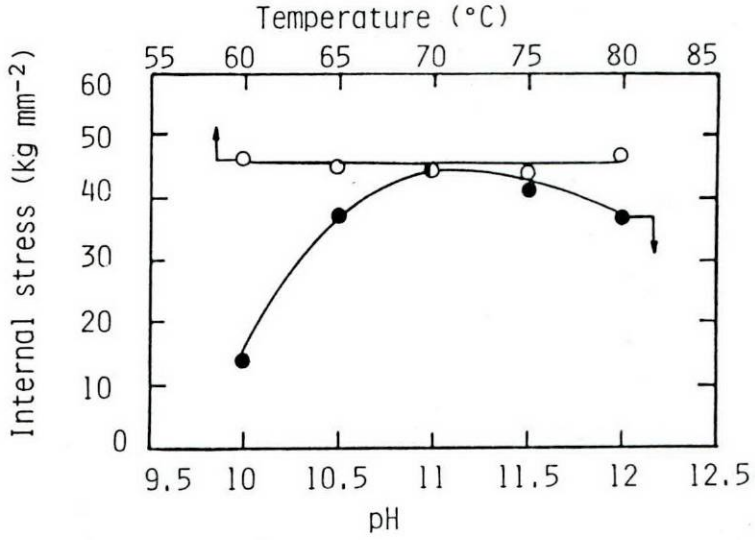

Fig.4 Effects of bath pH and temperature on the internal stress of Ni-P deposits

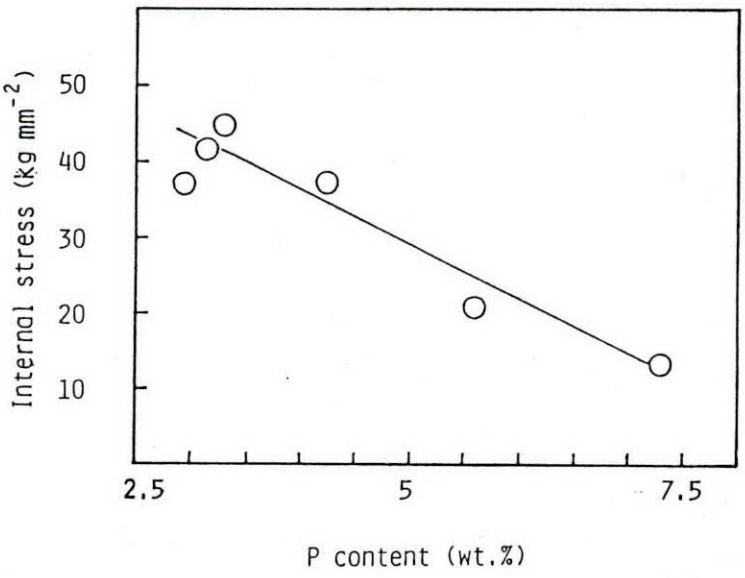

Fig.5 Effect of P content on the internal stress

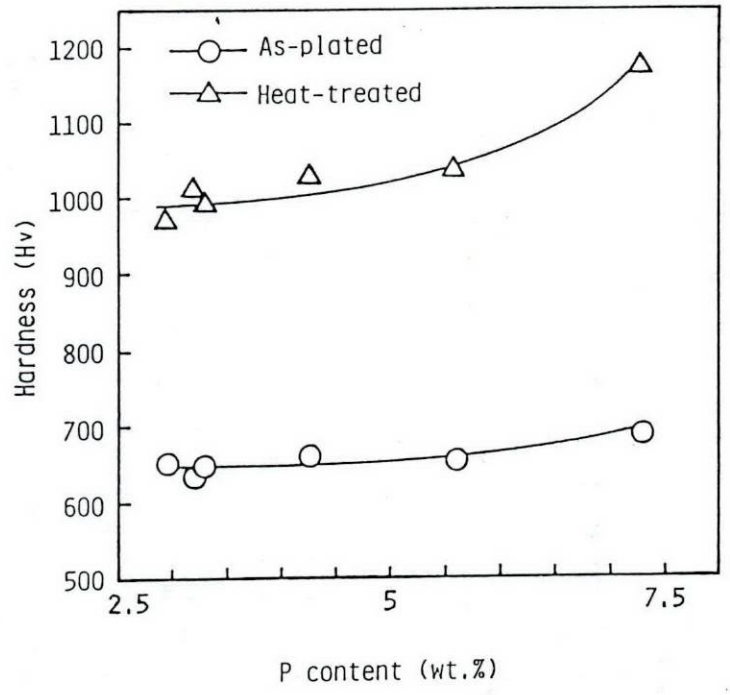

Fig.6 Effect of P content on the hardness of Ni-P alloys

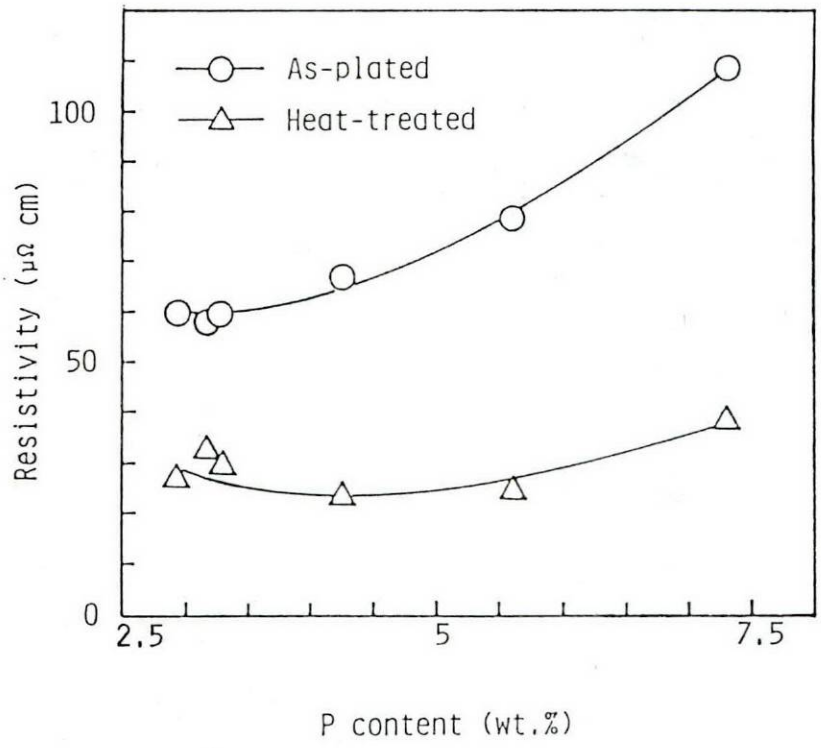

Fig. 7 Effect of P content on the resistivity of Ni-P alloys

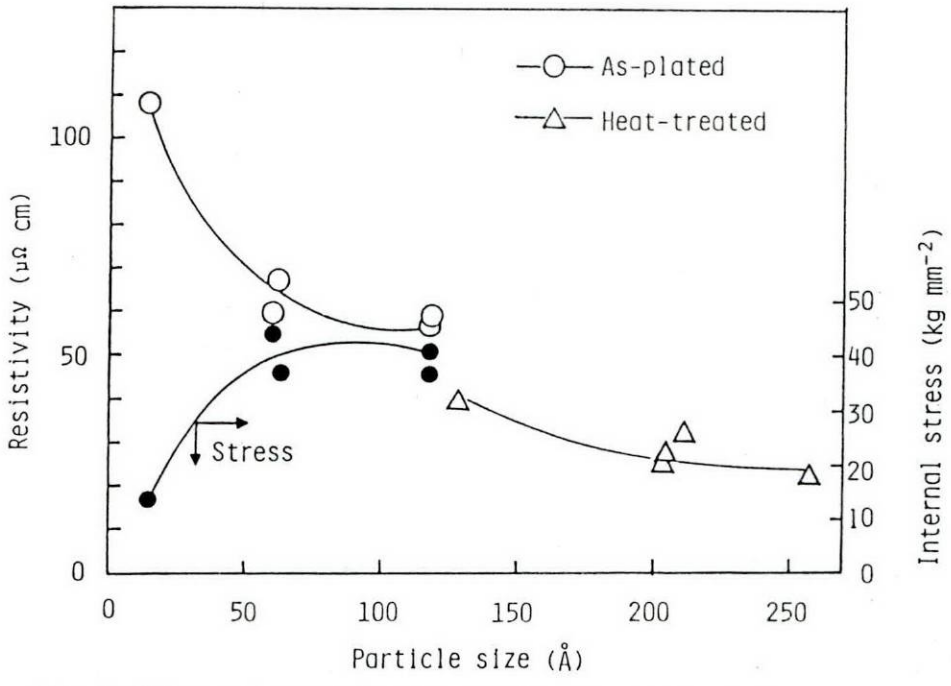

Fig. 8 Effect of particle size on the resistivity and internal stress of Ni-P alloys

I-6

Electroless Deposition I
Session I

Advanced Process Control Methods for Electroless Plating of Plastics

Gary Shawhan, Edwin Bastenbeck
and Richard Bellemare
Enthone, Inc.
350 Frontage Rd.
West Haven, CT 06516

ADVANCED PROCESS CONTROL METHODS FOR ELECTROLESS PLATING OF PLASTICS

Gary Shawhan, Edwin Bastenbeck, and Richard Bellemare
Enthone, Incorporated
350 Frontage Road
West Haven, Connecticut 06516

Abstract

The growth in requirements for electroless plating of plastics is focused on a wide range of engineering applications for such industries as computers, business equipment, automotive, aerospace, and military. The purpose of the electroless plating is most often for EMI shielding but may include other reasons such as lightning strike, electromagnetic pulsation protection, wear or abrasion resistance, etc. In all cases, the concern of the user is to provide a high quality product that can last for many years in the environment without loss of performance. Such failures can in fact lead to warrantee problems, and even leave the companies vulnerable to competition due to product failure.

The process for electroless plating of plastics is involved, but when properly operated with good control procedures, consistent and reproducible results with respect to adhesion can be attained. Currently, high volume production of structural foam and molded polycarbonate is being done for purposes of EMI shielding of computer enclosures for example. Industry requirements exist for accelerated temperatures humidity cycling have been established to test the durability of the coating. These requirements are revealing important differences in product quality (related to chemistry and molding) that may indicate where plated plastic parts can perform in service for extended warrantee periods without failure. Unfortunately, this method can take twenty days or more to determine possible failure.

This paper provides information on process control methods which can be employed to improve the consistency of plated plastics. Included among these methods is a new accelerated autoclave test method which allows rapid determination of early failures in temperature humidity and is well suited for on-line confirmation of product quality.

Introduction

The current use of electroless plating on structural foam and hardwall polycarbonate and polycarbonate blends for business equipment is intended to provide shielding from electromagnetic interference. Clearly from the standpoint of the manufacturer this protection from EMI needs to be capable of maintaining itself over the expectant service life and stated warrantee period of the equipment. Furthermore, during this period, the

integrity of the coating must be retained including its adhesion to the plastic substrate. Test procedures which can be correlated to prolonged service become an important consideration to simulate this longer term environmental period.

UL-746 Adhesion Testing

One standard used to evaluate the effect of the in-service environment on conductive coatings is UL-746C. This method, summarized in Table I outlines four separate conditions under which adhesion testing is performed according to ASTM Method D3359-83 (measuring adhesion by Tape Test). The criteria for evaluating adhesion of the plating to the plastic is based on a scribed cross-hatch pattern. The amount of plate removed after a specified tape is applied to this cross-hatched surface and then lifted off (in a designated manner) is assigned a rating according to the scale shown in Figure 1.

In the case of plated polycarbonate test results on actual production reveal generally consistent passes per UL-746C in the 4-5 range even with fairly wide swings in plating process chemistry. While this can be somewhat comforting to the design engineer in terms of the width of the operating window, several issues still remain as a concern. First, the correlation to actual service needs to be examined further. Second, the test method does not readily discern differences in process variables which might be expected to influence coating adhesion. In this instance, again, the value of the UL-746C method for determining long term equipment reliability must be questioned. The test matricies for two groups of plated polycarbonate, shown in Figure 2, illustrates this point.

Accelerated Temperature Humidity Testing

More recently, one equipment manufacturer instituted a test method based on temperature humidity cycling that has proven both more severe and more discerning in its ability to detect variations in coating quality and the related process conditions which produced it. This method, as outlined in Table II is referred to as the "4/4/16 Accelerated Temperature Humidity Test". At the present time, twenty (20) cycles of 4/4/16 testing is required after which a rating of 3B or higher is considered acceptable. Twenty cycles is also an attempt at correlating to five (5) years or more component service life and a better more rigorous means of assuring customer satisfaction beyond the warrantee period. Furthermore, ASTM is presently considering adoption of this test procedure for the purpose of evaluating the integrity of the plated plastic under accelerated aging conditions.

4/4/16 testing was conducted on plated structural foam and hardwall polycarbonate as indicated in a segment of the test results shown in Table III. This testing revealed significant inconsistencies in adhesion of the plated parts. In most cases, results fell far short of the required twenty cycles. Unfortunately, twenty cycles of 4/4/16 take twenty days to run. This does not include the time required to pull parts from the

line, arrange the shipment, plan testing and report the results. Therefore, the actual time involved before results might be available might be one to two months during which a lot of production could be processed and shipped and would require eventual return for reprocessing.

In today's climate of statistical process control, an essential component of process improvement is prevention before the fact, rather than detection of rejects after they are made. That is under "normal" quality control methods where testing is performed after the fact, the principles of SPC are violated. Obviously in this case, the use of the 4/4/16 test falls far short of providing the kind of timely on-line information necessary to insure the process is in control and capable of producing good parts.

Accelerated Autoclave Test Method

As a consequence of such field experiments, investigations were initiated into test methods which could be used on-line. The intention would be to provide more immediate information on coating adhesion and the control of the process as it related to the quality required by the user. These objectives clearly required careful development of the methodology. Several of the key objectives included:

General Objectives in Test Method Development

- Simple test method.
  - Low cost.
  - Small, adaptable to most facilities.
- Accelerated test with results available in the shortest time possible.
- Excellent correlation to the long term 4/4/16 temperature humidity test method.
- Suitability for inclusion into an SPC program.

Following several months of experimentation attempting to achieve these objectives, an autoclave procedure was developed that showed significant promise. As shown in Figure 3 adhesion tests performed on production structural foam polycarbonate showed very good correlation between autoclave testing and long term temperature humidity cycling. In fact, continued examination of test results began to establish a correlation between the number of cycles of 4/4/16 temperature humidity testing and single thirty minute autoclave tests. This is graphically represented by the statistical distribution curve in Figure 4.

The accelerated autoclave test method is performed according to the procedure outlined in Table IV. There are several important elements

in the successful implementation of the test method. First, samples need to be removed from the same section of the enclosure to insure that the most critical surfaces are being examined. In this case, the sprew area and gate area are typically the most significant surfaces requiring examination.

Adhesion Failure Mechanisms

The intention of this test method is to examine adhesion of the plated plastic. The various types of adhesion failures which can occur with plated polycarbonate include the three main mechanisms as illustrated in Figure 5. These include:

Failure Type	Source of Failure
Cohesive Failure	Over-etch of plastic resulting in degraded crumbled surface.
External Corrosive Failure	Moisture attack of the copper/substrate interface through porosity in the nickel.
Internal Corrosion	Chemicals or moisture left in the polycarbonate substrate plastic attacking the substrate/coating interface.

Comparison of 4/4/16 Testing to the Autoclave Method

In general, results from the autoclave temperature humidity test suggested 3-5 cycles could be equated to one thirty minute autoclave test. Furthermore, it was common that if the plated part passed two autoclave cycles (8-10 or more 4/4/16 cycles) it could be expected to pass over twenty cycles of 4/4/16 testing. Thus, one to two hours of on-line testing could be used to supplement (not replace) twenty days or more of extended testing in a full scale accelerated test.

Another important aspect to this type of accelerated testing is its ability to investigate various individual elements of the process. This can help isolate weak points in the process and provide a quantified performance result to identify process improvements. A good example of this approach is illustrated in the data presented in Figure 6. In this instance, we were studying the influence of post plate drying cycles on the adhesion of the plating. The intention was to identify the optimum drying technique and to identify a possible source of premature 4/4/16 adhesion failure on the finished part.

As can be seen by the information presented in Figure 6 air drying over a prolonged period of time clearly produces a poor adhesion result on polycarbonate. The one hour dry cycle followed by accelerated baking

produced the best results in this case. Based on these autoclave results and other tests process changes were implemented on the production line which significantly improved coating adhesion after 4/4/16 testing.

Process Control for Plated Plastics

In the broader perspective of today's marketplace process technology, such as that represented by the field of conductive coatings, is undergoing a re-evaluation. The re-evaluation is focused on the fundamental issues of statistical process control (SPC) and statistical quality control (SQC). From the perspective of today's user the selection of conductive coatings must be based on the predictability of its performance, an expectation of consistent quality and the assurance of stable, competitive costs. This cost optimization is achieved primarily from refinements in the process resulting in icreased output and the elimination of scrap. The concept is simple and well known. **Prevention** by process control instead of detection by quality control after the rejects have been made. The advancement of plated plastics particularly for applications such as EMI shielding which services industries heavily involved in SPC programs in essence is predicated on improvements in all of these areas. It is not only desireable for applicators of plated plastics to consider these concepts, it is becoming manditory that established programs be in place. In one sense failure to do so can dictate the selection of one supplier over another. In an even more serious scenario it can dictate a switch to alternate coating technology.

The availability of the accelerated autoclave temperature humidity test is an important tool for plated polycarbonate moldings in helping to meet these objectives. This is especially true in that adjustments in individual elements in the process can be studied with almost immediate feedback on the improvements they might represent in final product quality. This clearly allows tighter control limits to be set on each element of the chemical process and allows the applicator to strive for a defect-free operation.

In an effort to advance plating on plastics technology toward the ultimate goal of defect-free output, statistical process control has been initiated in production. This strategy has followed the basic principles of SPC as outlined in Table V. Our first objective was to try to bring each step of the process in control and eliminate special causes, as graphically illustrated in Figure 7. Second, through the gathering of statistics it was our intention to determine the capability of the process to meet the customer requirements. Then through fine tuning the chemistry we wanted to insure that we could maintain each element of the process within necessary control limits, i.e. establish capability. This concept is illustrated in Figure 8. In most all cases, a control chart format is used as part of establishing a program for controlling the process and improving its capability. An example of this approach is given in Figure 9 whereby you can see the upper and lower control limits, as well as the optimum value (x). Tests are run on each parameter are considered

important to the particular process solution and plotted out an on-going basis. In production, once the proper routine was established for doing the analysis, making timely chemical additions and recording the results, improvements were obvious in product quality and resulting yield.

Summary

In summary, the accelerated autoclave temperature humidity test offers an important diagnostic tool for studying the plating on plastics product. The fact that this method is under consideration for adoption by ASTM adds to its importance in this regard. Furthermore, its correlation to long term, established industry testing appears very good based on current work with structural foam and hardwall polycarbonate.

Information developed from the accelerated test method has contributed greatly to the cause of studying individual process variables and establishing an SPC program. The ready adaptability of plated plastics to statistical process control methodology should increase the quality of plated product, reduce rejects and ultimately yield an optimal cost per unit.

The validity of this test method for examination of other plastic has not yet been demonstrated in relation to other accelerated tests such as the 4/4/16 method. Further work will be required on each plastic to determine its suitability for use with the accelerated autoclave method.

TABLE I

UL-746C ADHESION TEST METHOD SUMMARY

CRITERIA: <5% COATING REMOVAL BY TAPE TEST METHOD ASTM D 3359-83

TEST CONDITION:

1) **AS RECEIVED**
2) **AFTER AGING AT 85°C FOR 56 DAYS**
3) **AFTER AGING AT 35°C ± 2°C AND 90 ± 5% RELATIVE HUMIDITY FOR 56 DAYS**
4) **AFTER THERMAL CYCLE TESTING; 1 HOUR AT 85°C; PLUS 1 HOUR AT 23°C; PLUS 1 HOUR AT 23°C**

TABLE II

ACCELERATED TEMPERATURE HUMIDITY TEST METHOD (4 / 4 / 16)

CRITERIA: 3B OR HIGHER RATING AFTER 20 CYCLES; EACH CYCLE EQUATES TO 24 HOURS

TEST CONDITION:

a) **DWELL 4 HOURS AT 25°C ± 2°C; 47.5% ± 2.5% RELATIVE HUMIDITY**

b) **RAISE TEMPERATURE OVER 2 HOURS TO + 66°C ± 2°C; RAISE RELATIVE HUMIDITY TO 92.5% ± 2.5%**

c) **DWELL AT ABOVE CONDITIONS FOR 4 HOURS**

d) **HOLD TEMPERATURE AT +66°C ± 2°C; COVER RELATIVE HUMIDITY TO 47.5% ± 2.5%**

e) **DWELL AT ABOVE CONDITIONS FOR 11 HOURS**

f) **LOWER TEMPERATURE OVER 2 HOUR PERIOD TO 25°C ± 2°C; MAINTAIN RELATIVE HUMIDITY AT 47.5% ± 2.5%**

g) **RECYCLE**

TABLE III

4 / 4 / 16 TEMPERATURE HUMIDITY TESTING OF PLATED POLYCARBONATE

RUN#	PROCESS CONDITION	4 / 4 / 16 TEST RESULTS		
		2 CYCLES	6 CYCLES	9 CYCLES
1	STD CYCLE	2	-	-
2	STD CYCLE	1	-	-
3	STD CYCLE	4	1	-
4	STD CYCLE	4	1	-
5	STD CYCLE	4	1	-
6	STD CYCLE	5	4	4
7	STD CYCLE	5	4	4
8	STD CYCLE	5	3	3

TABLE IV

ENTHONE ACCELERATED TEMPERATURE / HUMIDITY AUTOCLAVE TEST PROCEDURE FOR PLATED POLYCARBONATE

APPARATUS REQUIRED: 1 AUTOCLAVE

1 STEREOCLAVE
ELECTRIC / AUTOCLAVE
VWR CAT. NO. 58617-006

PROCEDURE: * PRIOR TO TESTING, PANELS SHOULD BE AGED FOR MAXIMUM ADHESION BY BAKING AT APPROXIMATELY 170°F FOR 30 MIN. THEN ALLOWED TO AIR COOL TO ROOM TEMPERATURE

1) HEAT AUTOCLAVE TO BOILING
2) PLACE THE PANELS VERTICALLY IN THE AUTOCLAVE ABOVE THE SURFACE OF THE WATER
3) CLOSE THE AUTOCLAVE AND ALLOW TO REACH PRESSURE (12 PSI)
4) HOLD PRESSURE FOR 30 MIN.
5) AFTER 30 MIN., RELIEVE THE PRESSURE, REMOVE THE PANELS AND ALLOW THEM TO EQUILIBRATE TO ROOM TEMPERATURE FOR 1/2 HOUR
6) PERFORM ASTM CROSS HATCH ADHESION TEST AND RATE ACCORDINGLY
7) REPEAT STEPS 2 THRU 6 AS REQUIRED

TABLE V

PRINCIPLES OF SQC / SPC

- SET QUALITY STANDARDS / REQUIREMENTS
- ESTABLISH PROCESS CAPABILITY
- COMPARE CAPABILITY WITH REQUIREMENTS
- MONITOR THE PROCESS
- MAKE CORRECTIONS TO MAINTAIN PROCESS CONTROL

FIGURE 1

ASTM D 3359-83 CLASSIFICATION OF TAPE ADHESION RESULTS

CLASSIFICATION	SURFACE OF CROSS-CUT AREA FROM WHICH FLAKING HAS OCCURED. (EXAMPLE FOR SIX PARALLED CUTS)
5B	NONE
4B	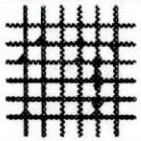
3B	
2B	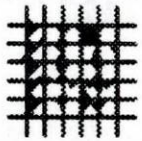
1B	
0B	GREATER THAN 65%

FIGURE 2

TYPICAL UL-746C ADHESION TEST RESULTS

RUN#	CONDITION	UL-746C TEST TEST CONDITION #1 AS RECEIVED	UL-746C TEST TEST CONDITION #3 HUMIDITY CYCLING
1	STD CYCLE	4-5B	4-5B
2	STD CYCLE	4B	4-5B
3	STD CYCLE	4-5B	4-5B
4	STD CYCLE	5B	5B
5	STD CYCLE	4-5B	4-5B
6	STD CYCLE	5B	5B
RUN#			
1	DRYING SEQUENCE A	5B	5B
2	DRYING SEQUENCE B	4-5B	4-5B
3	DRYING SEQUENCE C	4-5B	5B
4	DRYING SEQUENCE D	5B	5B
5	DRYING SEQUENCE E	4-5B	4-5B
6	DRYING SEQUENCE F	4-5B	4-5B

FIGURE 3

COMPARISON OF 4/4/16 AND AUTOCLAVE TEMPERATURE HUMIDITY TEST RESULTS ON PLATED POLYCARBONATES

RUN# FOAMED POLY-CARBONATE	4/4/16 TEST RESULTS	INITIAL RESULTS	1ST AUTOCLAVE	2ND AUTOCLAVE	3RD AUTOCLAVE	4TH AUTOCLAVE	5TH AUTOCLAVE
1	FAILED BY 3 CYCLES	3-4B	2-3B	2B	2B	1-2B	1-2B
2	FAILED BY 3 CYCLES	5B	2B	1-2B	1B	0B	0B
3	FAILED BY 20 CYCLES	5B	5B	3-4B	3B	3B	3B
4	FAILED BY 20 CYCLES	5B	5B	4-5B	4B	3B	3B
5	FAILED BY 20 CYCLES	5B	5B	5B	4-5B	3-4B	3B
6	FAILED BY 20 CYCLES	5B	5B	5B	5B	3-4B	3-4B
7	FAILED BY 15 CYCLES	5B	5B	4B	5B	2B	3B
HARDWALL POLY-CARBONATE							
1	PASSED 20 CYCLES	5B	5B	5B	5B	5B	5B
2	PASSED 20 CYCLES	5B	5B	5B	5B	5B	5B

FIGURE 4
RELATIONSHIP BETWEEN ONE-30 MUNUTE AUTOCLAVE TEST AND THE NUMBER OF 4/4/16 TEST CYCLES FOR PLATED POLYCARBONATE

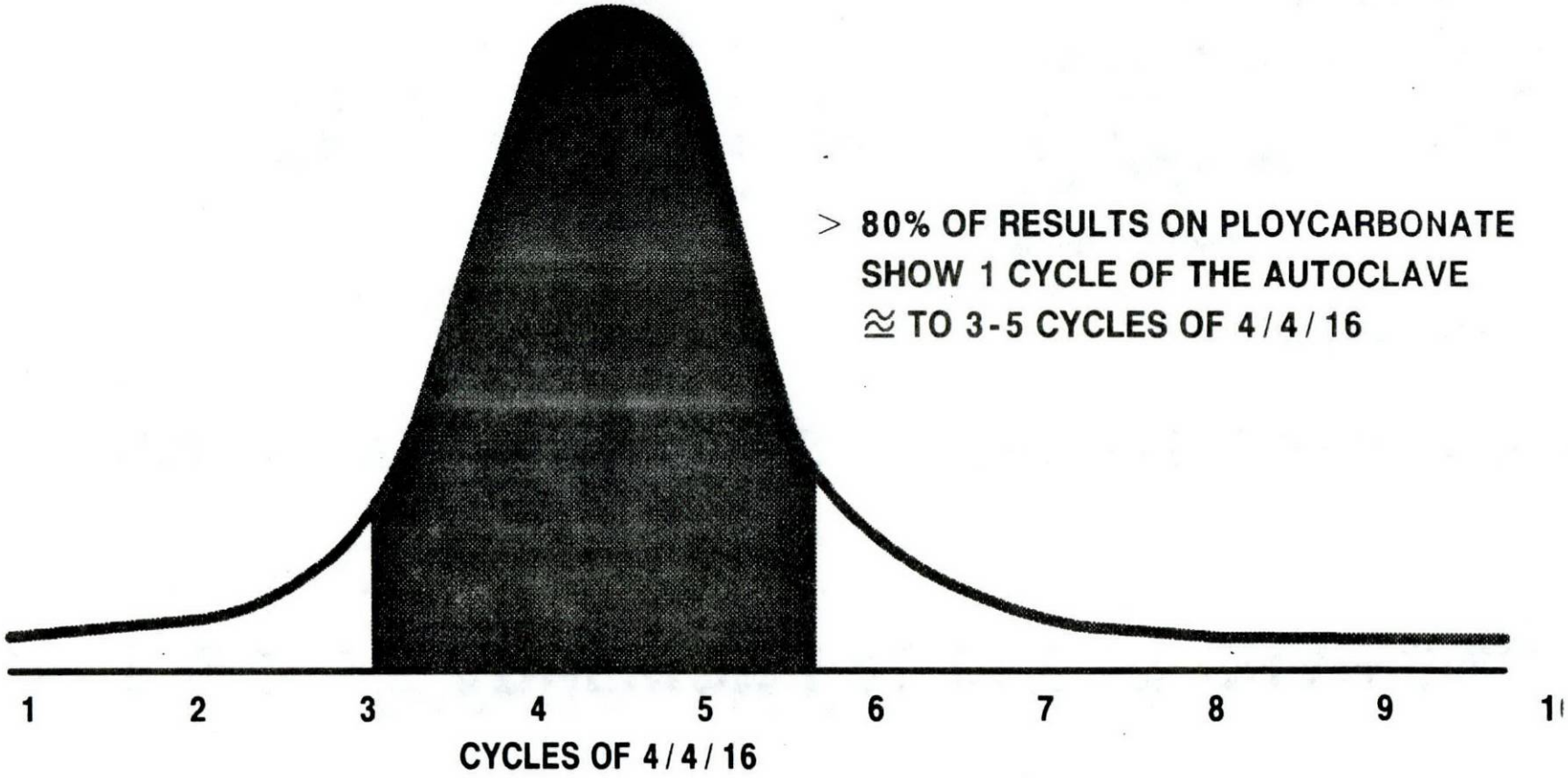

FIGURE 5 ADHESION FAILURE MECHANISMS

CORROSION FAILURE MODES

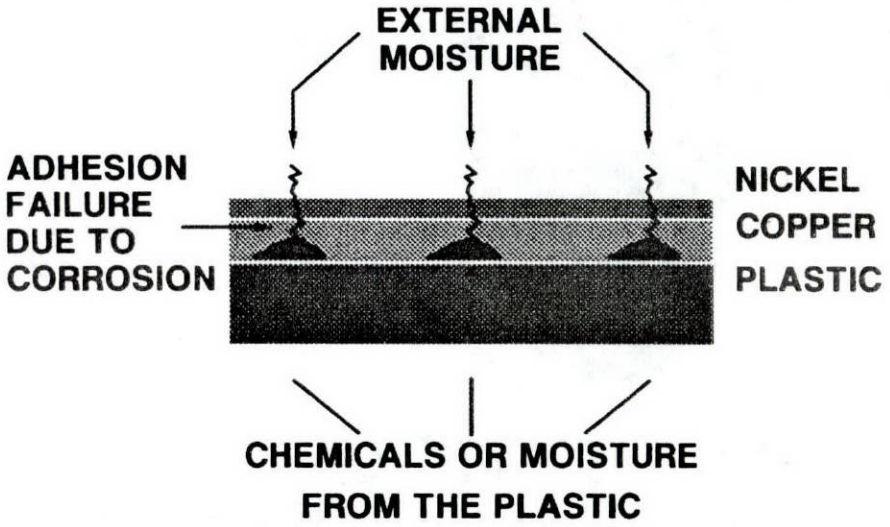

COHESIVE FAILURE MODE

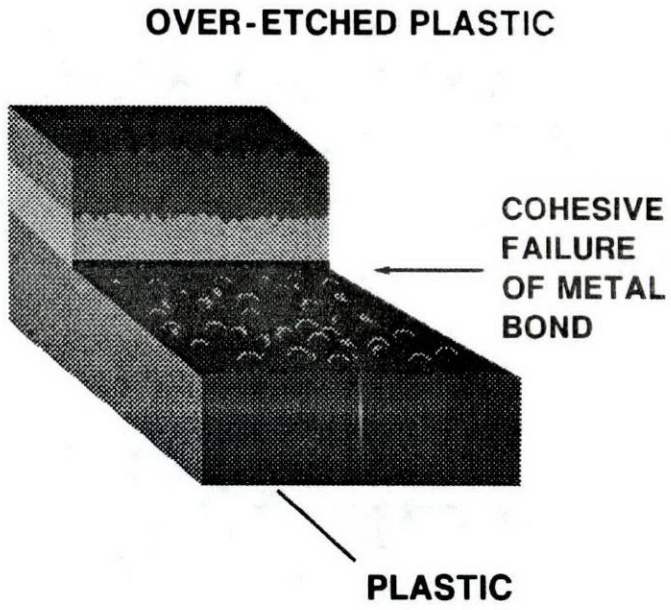

FIGURE 6

EXAMINATION OF VARIOUS POST-PLATE DRYING CYCLES USING THE ACCELERATED AUTOCLAVE TEST METHOD

TAPE TEST

TEST CONDITION	INITIAL RESULTS	1ST AUTOCLAVE	2ND AUTOCLAVE	3RD AUTOCLAVE	4TH AUTOCLAVE	
AIR DRY WITH EXTENDED TIME DELAY (NO BAKE)	4B	■	1B	0B	0B	
EXTENDED DRY IN AIR EXTRA POST RINSE (BAKE 25 MIN)	5B	5B	5B	■	2B	
IMMEDIATE DRYING AFTER RINSE (NO BAKE)	5B	5B	4B	■	2B	
AIR DRY 1 HR, (BAKE 25 MIN)	5B	5B	5B	5B	4B	PASS

■ FAILURE POINT (<3B)

FIGURE 7

PROCESS CONTROL

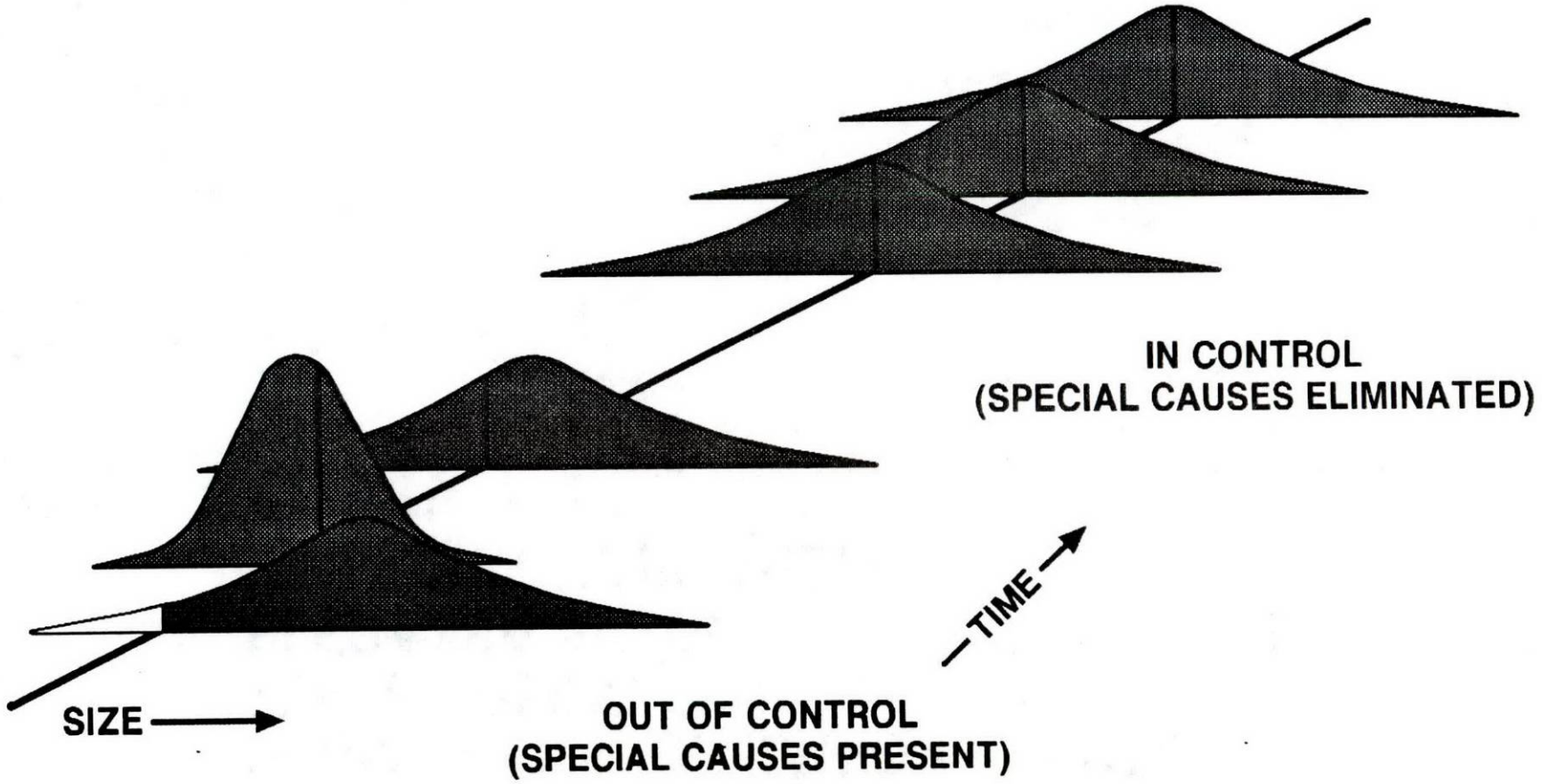

FIGURE 8

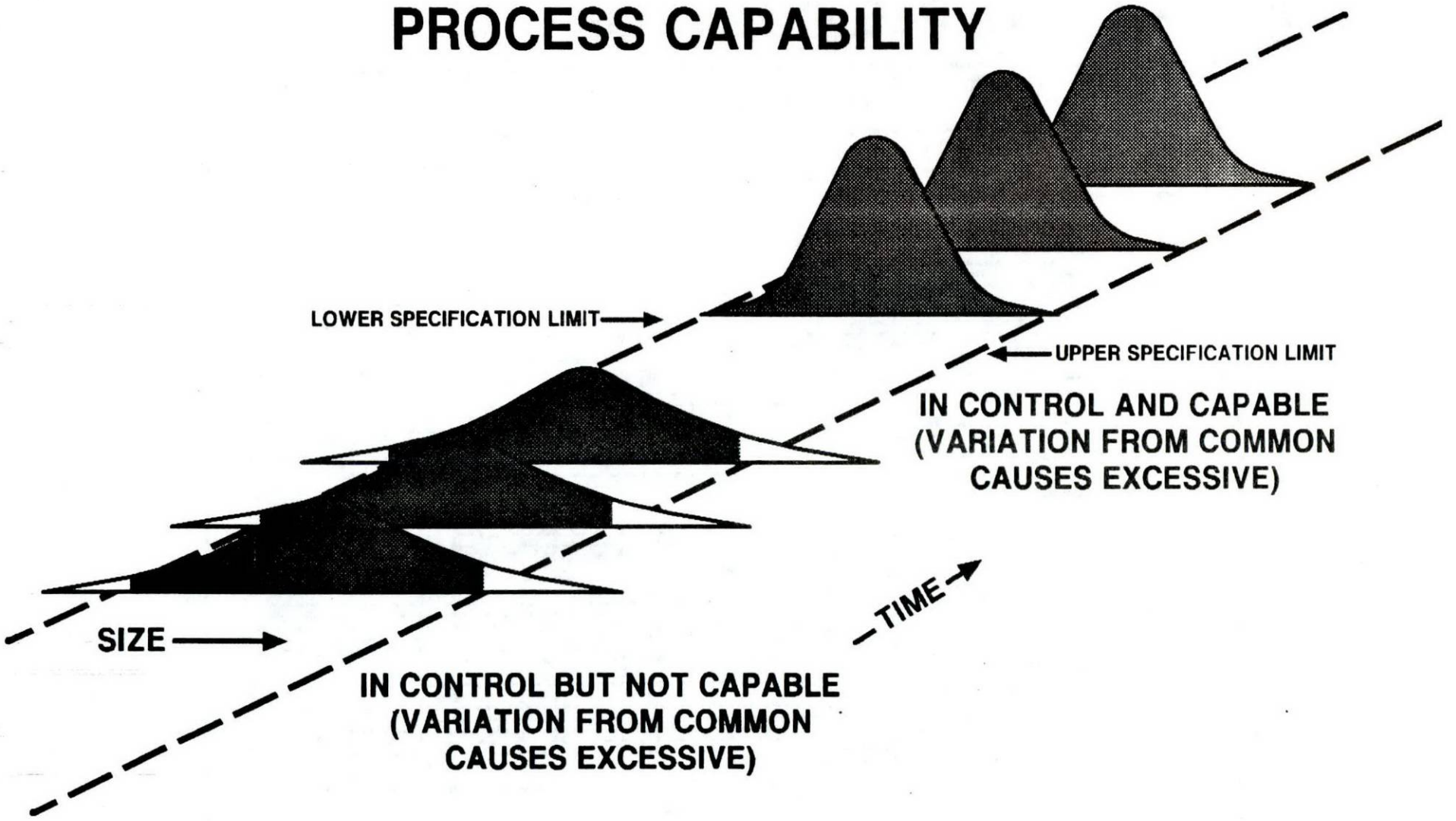
PROCESS CAPABILITY
LOWER SPECIFICATION LIMIT
UPPER SPECIFICATION LIMIT
IN CONTROL AND CAPABLE
(VARIATION FROM COMMON
CAUSES EXCESSIVE)
SIZE
TIME
IN CONTROL BUT NOT CAPABLE
(VARIATION FROM COMMON
CAUSES EXCESSIVE)

FIGURE 9 SAMPLE CONTROL CHART

COMPANY	LINE	RACK	PROCESS ELECTROLESS COPPER	TEST FREQUENCY 2 HRS.	PART NO.	REPORT NO.
JOB NO.	DATES		TEST PH OF SOLUTION			

